Tire/road contact modelling for a rolling tire

Kersjes, S.H.M.

Award date:
2006

Tire/road contact modelling for a rolling tire

DCT 2006.66

July 17, 2006
Eindhoven University of Technology (TU/e)

S.H.M. Kersjes s0550169 (TU/e)

Supervisors: Dr. Ir. I. Lopez Arteaga (TU/e)
Dr. Ir. A.J.C. Schmeitz (TU/e)
Prof. Dr. Ir. N.B. Roozen (TU/e)
Prof. Dr. H. Nijmeijer (TU/e)

To my dear friend Tim
1982 - 2005

Samenvatting

Tegenwoordig wordt verkeersgeluid een steeds groter probleem in druk bevolkte gebieden, des te meer omdat in de toekomst de regelgeving omtrent omgevingsgeluid strenger wordt. Een van de belangrijkste problemen, vooral boven snelheden van 50 km/h, is het bandengeluid dat overheerst bij deze snelheden. Onderzoek toont aan dat voor frequenties tot en met 1 kHz, bandvibraties de dominerende geluidsbron zijn. Deze bandvibraties ontstaan door de (contact) interactie tussen band en wegdek. Om deze trillingen te kunnen voorspellen, en zo het ontwerp van banden te verbeteren, is een band-vibratiemodel nodig.

In 2005 is een modaal gebaseerd vibratiemodel ontwikkeld op de Technische universiteit Eindhoven, welke de Doppler-verschuiving door rotatie van de band meeneemt. De volgende stap in dit onderzoek, en het doel van dit master project, is het verbeteren van de efficiëntie van het model en het implementeren van een contactmodel tussen de band en het wegdek. Dit contactmodel moet de krachten tussen band en wegdek kunnen bepalen terwijl de band over het wegdek rolt.

Omdat in een dynamische simulatie de distributie van contactpunten continue verandert in de tijd, is de interactie tussen band en wegdek niet-linear. Door deze niet-lineariteit moet het contactprobleem worden opgelost in het tijddomein. De responsie van de band wordt daarom bepaald met het convolutie product tussen de Green's functies en de contactkrachten. Om de efficiëntie van het model te verbeteren is een semi-analytische uitdrukking afgeleid voor het uitrekenen van deze Green's functies. Deze uitdrukking is gevonden door de set van vergelijkingen die het systeem beschrijft te ontkoppelen. Om het probleem van niet diagonale en niet symmetrische matrices op te lossen, is het probleem herschreven als een één dimensionaal probleem en is het eigenwaardeprobleem voor een tweede keer opgelost.

Om een contactmodel te vinden is literatuuronderzoek gedaan; hieruit blijkt dat voor het berekenen van de verticale krachten een oneindig halfvlak het beste gebruikt kan worden. Voor de horizontale krachten zal een discreet borstelmodel worden gebruikt, zonder stick/slip. Om het contactprobleem op te lossen is het probleem gedefinieerd als een beginwaardeprobleem. Dit probleem bevat de responsie van de band als gevolg van de contactkrachten, de contactkrachten zijn zodoende gekoppeld aan de bandresponsie.

Simulaties met het model laten zien dat het model goed overeenkomt met simulaties gedaan met het eindige elementen pakket Abaqus. Ook de invloed van het aantal gebruikte modes is onderzocht. Dit laat zien dat er een grote hoeveelheid modes mee moet worden genomen om de responsie correct te modelleren. De gepresenteerde resultaten laten zien dat het model dezelfde effecten laat zien als die gevonden worden in literatuur. Hierdoor is een gevalideerd model verkregen dat dezelfde resultaten laat zien als in de literatuur.

Abstract

Nowadays traffic noise is becoming an increasingly big problem in densely populated areas, especially since in the future environmental noise regulations become more strict. One of the main problems in traffic noise, mostly above vehicle speeds of 50 km/h, is the tire/road noise which prevails at these speeds. Research has shown that for frequencies up to 1 kHz, tire vibrations are the most dominant noise source. These tire vibrations are caused by the (contact) interaction between tire and road. In order to be able to predict the tire vibrations, and in that way improve tire design, a tire/road vibration model is needed.

In 2005 a modal based tire vibration model is developed at the Eindhoven University of Technology, including the Doppler shift due to tire rotation. The next step in this research, and the aim of this master project, is to improve the computational efficiency of the tire model and implementing a tire/road contact model. This tire/road contact model must be able to calculate the forces originated at the tire/road contact under rolling conditions.

Since in a dynamic simulation, the distribution of contact points constantly changes in time, the tire/road interaction is non-linear. Due to this non-linearity the contact problem has to be solved in the time domain. The response of the tire to the contact forces is therefore obtained from the convolution product of the Unit Time Response functions (Green's functions) and the contact forces. To improve computational efficiency, a semi-analytical expression is created for the calculation of these Green's functions. This expression is found by decoupling the set of equations describing the system. To overcome the problem of non-diagonal and non-symmetric matrices the system is rewritten as a one dimensional problem and the eigenvalue problem is solved a second time.

To find a contact model a literature study has been performed, which pointed out that an elastic half-space is the best vertical contact model for this research. The horizontal contact forces are included using a discrete brush model without stick/slip. To solve the contact problem it is transformed to an initial value problem. This problem includes the response of the tire due to the calculated contact forces, thus the contact forces are coupled with the response of the tire.

Validation of the model shows that the model correlates well with simulations done in the finite element package Abaqus. Also the dependency of the number of modes is investigated, where it is shown that a large number of modes has to be taken into account to represent the correct behavior. The presented results show that the model includes the effects in the contact patch, that are presented in literature. Hence, a validated model is obtained, which shows the same effects as discussed in literature.

Contents

List of Symbols

Symbol	Definition	Unit
a	Size pressed area of the elastic half-space x-direction	[m]
b	Size pressed area of the elastic half-space y-direction	[m]
$\mathbf{C}$	Influence matrix elastic half-space	
$\mathbf{D}$	Damping matrix	
$\mathbf{D}_{mod}$	Modal damping matrix	
$\tilde{\mathbf{D}}$	Modal damping matrix, in the reference frame	
$\vec{\mathbf{e}}^1$	Fixed reference coordinate system	[-]
$\vec{\mathbf{e}}^2$	Body fixed coordinate system	[-]
E	Young's modulus, elastic half space	[MPa]
F	Force	[N]
$\mathbf{f}$	Force vector	
$\tilde{\mathbf{f}}$	Vector containing modal excitation forces	
g	Green's function	[m/N]
$\mathbf{H}$	Transfer function matrix	
K_b	Brush stiffness, brush model	[N/m]
$\mathbf{K}$	Stiffness matrix	
$\mathbf{K}_{mod}$	Modal stiffness matrix	
$\tilde{\mathbf{K}}$	Modal stiffness matrix, in the reference frame	
m	Number of modes	[-]
$\mathbf{M}$	Mass matrix	
$\tilde{\mathbf{M}}$	Modal mass matrix, in the reference frame	
n	Number of dofs	[-]
n_k	Number of circumferential waves	[-]
N	Time increment	[-]
p	Contact pressure	[Pa]
r_e	Effective rolling radius	[m]
s	Eigenvalue, second eigenvalue problem	
t	Time	[s]
u	Displacement	[m]
$\mathbf{u}$	Displacement vector	
$\mathbf{V}$	Diagonal matrix containing eigenvalues	
$\mathbf{U}$	Matrix containing the eigenvectors of the second, right, eigenvalue problem	
$\mathbf{W}$	Matrix containing the eigenvectors of the second, left, eigenvalue problem	
x	X position in the elastic half-space	[m]
y	Y position in the elastic half-space	[m]
z	Vertical position	[m]
$\mathbf{z}$	vector containing initial coordinates	

List of symbols continued...

Symbol	Definition	Unit
α	Angular position in the body fixed frame	[rad]
β	Angular position in the reference frame	[rad]
γ_1	Rayleigh damping coefficient (mass)	[Ns/(mkg)]
γ_2	Rayleigh damping coefficient (stiffness)	[s/kg]
Φ	Modes	[-]
$\boldsymbol{\eta}$	Modal displacement vector	
λ	Eigenvalue, first eigenvalue problem	
ν	Poisson ratio elastic half-space	[-]
ξ	Damping factor brush model	[-]
ρ	Density	[kg/m^3]
ψ	Potential	
ω	Frequency	[rad/s]
Ω	Rotational speed	[rad/s]
Δt	Time step	[s]
$\mathbf{\Pi}$	Vector containing the initial value problem	

Chapter 1

Introduction

1.1 Motivation and background

Nowadays traffic noise is becoming an increasingly big problem in densely populated areas, especially since in the future environmental noise regulations will become more strict. One of the main problems in traffic noise, mostly above vehicle speeds of 50 km/h, is the tire/road noise which dominates at these speeds. With respect to interior noise, to which the occupants of the vehicle are exposed, tire/road noise is becoming more and more important. This is a consequence from the fact that automotive engine noise and other mechanical noise become increasingly more silent. Especially with the trend towards hybrid-electrical cars. Therefore tire/road noise is a problem which has to be tackled, thus making an interesting field of research.

In order to reduce the tire/road noise a deep understanding of the noise generation mechanisms is of great importance. In the last 30 years extensive research is performed with regard to the different noise generation mechanisms, in which it is shown that for frequencies up to 1 kHz tire vibrations are the most dominant noise source. With respect to interior noise, tire vibrations are the most important source of noise. Tire vibrations up to 500 Hz are transmitted via structural transmission paths to the interior effectively, thus causing acoustic noise. The cause of tire vibrations is the (contact) interaction between tire and road. Here each non-uniformity, as road roughness or non-roundness, will excite the tire. In order to be able to predict the tire vibrations, and in that way improve tire design, a tire/road vibration model is needed. When constructing such a model one of the most important, but likely the most difficult, subject is to model the contact forces correctly.

The research on tire/road modelling at Eindhoven University of Technology started in 2004. Blom [2005] developed a modal based tire vibration model, including the Doppler shift due to tire rotation. This model is valid in the 0-500 Hz region, which is the region of interest with respect to interior noise. It also appeared to be a region where few models are available. The next step in this research is to model the interaction between tire and road in order to determine the forces acting on the tire.

1.2 Aim and scope

The aim of this master thesis is to extend the work started by Blom [2005] by improving the computational efficiency of the tire model and implementing a tire/road contact model. This tire/road contact model must be able to calculate the forces originated at the tire/road contact under rolling conditions.

1.3 Contents of this report

First in chapter 2, the tire model presented by Blom [2005] is discussed. Hereafter, in chapter 3 a literature study is presented where different contact models are discussed and a conclusion is drawn about which model can be implemented best. In chapter 4, a semi-analytical expression of the unit impulse response function (Green's function) for a rotating tire is derived. This has improved the computational efficiency of the tire model significantly. The contact model and its use is discussed in chapter 5. Some validation work, with finite element simulations, is described in chapter 6 to indicate that the theory and its implementation are correct. In chapter 7, some results of the model are presented and discussed. Finally, in chapter 8 conclusions are given and recommendations for further research are formulated.

Chapter 2

Tire/road model

In this chapter it is discussed how the tire/road model is build and which functions are used. Before explaining the tire/road model, first some attention will be given on how the tire vibration model works, since this is the center part of the calculations.

2.1 Tire vibration model

The tire vibration model used in this research is the modal tire model created by Blom [2005]. This model takes into account the tire rotational velocity and divides the contact problem into two parts to include the nonlinear tire deformation behavior. In this section the model and the used approach will be discussed.

2.1.1 Modal tire model (Blom [2005])

Blom [2005] concluded that using a modal approach to calculate the time domain response of a tire may be a computational cheap approach. By initially deforming the tire in a static FE simulation, the large and non-linear deformation of the tire is determined using the full system of equations. Subsequently, the modal base is constructed around this static state, thus incorporating the effect of tire/road contact. The dynamic response of the tire due to road roughness is then calculated using the modal superposition principle. To take into account the effect of rotation two coordinate systems are used: $\vec{\mathbf{e}}^1$ and $\vec{\mathbf{e}}^2$. $\vec{\mathbf{e}}^1$ is the reference coordinate system that is fixed to the center of the tire and translates together with the tire, but does not rotate. $\vec{\mathbf{e}}^2$ is a body-fixed coordinate system. This means that this system rotates with the tire at velocity Ω, see figure 2.1. In these systems the angles α (in the body-fixed frame) and β (in the reference frame) are defined so that for a certain point k on the tire $\beta_k = \alpha_k + \Omega t$. In the explanation of the model used here, the excitation is defined as a point force acting at a fixed point in the reference frame. This leads to the following system of equations describing the tire in a fixed reference frame (see Blom [2005]):

$$\tilde{\mathbf{M}}\ddot{\boldsymbol{\eta}}(t) + \tilde{\mathbf{D}}\dot{\boldsymbol{\eta}}(t) + \tilde{\mathbf{K}}\boldsymbol{\eta}(t) = \tilde{\mathbf{f}}(t) \tag{2.1}$$

with $\tilde{\mathbf{M}}$ the modal mass matrix, $\tilde{\mathbf{D}}$ the modal damping matrix, $\tilde{\mathbf{K}}$ the modal stiffness matrix, $\boldsymbol{\eta}$ the modal coordinates and $\tilde{\mathbf{f}}$ the modal excitation force. The matrices are defined as follows:

$$\tilde{\mathbf{M}}_{mxm} = \mathbf{I} \tag{2.2}$$

$$\tilde{\mathbf{D}}_{mxm} = 2\mathbf{P}(\Omega, \mathbf{M}, \boldsymbol{\Phi}) + \mathbf{D}_{mod} \tag{2.3}$$

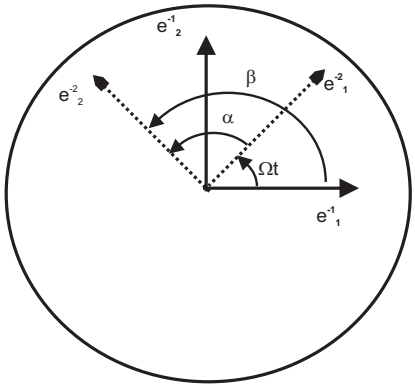

Figure 2.1: Coordinate system.

$$\mathbf{D}_{mod} = \mathbf{\Phi}^T \mathbf{D} \mathbf{\Phi} \tag{2.4}$$

$$\tilde{\mathbf{K}}_{mxm} = \mathbf{S}(\Omega, \mathbf{M}, \mathbf{\Phi}) + \mathbf{D}_{mod}\mathbf{P}(\Omega, \mathbf{M}, \mathbf{\Phi}) + \mathbf{K}_{mod} \tag{2.5}$$

where m is the number of modes included and,

$$\mathbf{P}(\Omega, \mathbf{M}, \mathbf{\Phi}) = \mathbf{\Phi}_{rf}^{1T}(\beta)\mathbf{M}_{rf}^{1}\left(\hat{\mathbf{\Omega}}\mathbf{\Phi}_{rf}^{1}(\beta) + \Omega\frac{\partial \mathbf{\Phi}_{rf}^{1}(\beta)}{\partial \beta}\right) \tag{2.6}$$

$$\mathbf{S}(\Omega, \mathbf{M}, \mathbf{\Phi}) = \mathbf{\Phi}_{rf}^{1T}(\beta)\mathbf{M}_{rf}^{1}\left(\hat{\mathbf{\Omega}}^2\mathbf{\Phi}_{rf}^{1}(\beta) + 2\Omega\hat{\mathbf{\Omega}}\frac{\partial \mathbf{\Phi}_{rf}^{1}(\beta)}{\partial \beta} + \Omega^2\frac{\partial^2 \mathbf{\Phi}_{rf}^{1}(\beta)}{\partial \beta^2}\right) \tag{2.7}$$

$$\hat{\mathbf{\Omega}} = \begin{pmatrix} 0 & \Omega \\ -\Omega & 0 \end{pmatrix} \tag{2.8}$$

In the above equations $\mathbf{\Phi}$ is the matrix of eigenvectors determined in Abaqus, where the subscript rf indicates that reference frame fixed modes are used. Ω is the rotational velocity of the rotating reference frame (note that this a constant value). β the angle between the reference fixed and body fixed frame. $\mathbf{M}$, $\mathbf{D}$, and $\mathbf{K}_{mod}$, are the mass matrix, damping matrix and a diagonal matrix containing the squares of the eigenfrequencies (calculated in Abaqus) respectively. The mass matrix is created using the mass distribution of a single segment of the tire model. By assuming that the weight distribution is equal for al the segments, the global mass distribution is found. Hence the constructed mass matrix is a lumped mass matrix. The damping matrix $\mathbf{D}$ is calculated assuming Raleigh damping $\mathbf{D} = \gamma_1\mathbf{M} + \gamma_2\mathbf{K}$. Due to the effect of rotation the matrices $\tilde{\mathbf{D}}$ and $\tilde{\mathbf{K}}$ are non-diagonal and non-symmetric, which means that the set of modal coordinates $\boldsymbol{\eta}(t)$ is not a set of modal coordinates for the rotating tire. Therefore the eigenfrequencies in $\mathbf{K}_{mod}$ are not the eigenfrequencies of the rotating tire. A second eigenvalue problem should be solved in order to determine the eigenfrequencies and mode shapes of the rotating tire.

2.1.2 Used FE Model

The FE tire model in this research is a rubber torus as displayed in figure 2.3, which is a very simplified model of a real tire. The model consists of only one layer of rubber and has no reinforcement as is shown in figure 2.2. The parameter values have been estimated in such a way that the first resonance

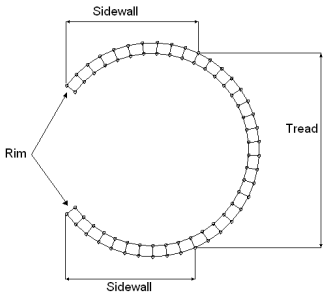

Figure 2.2: Cross section torus.

frequency is approximately equal to the first resonance of a real tire (Blom [2005]). This is however no problem because the model is only used to test the theory. The parameters can be found in appendix B.

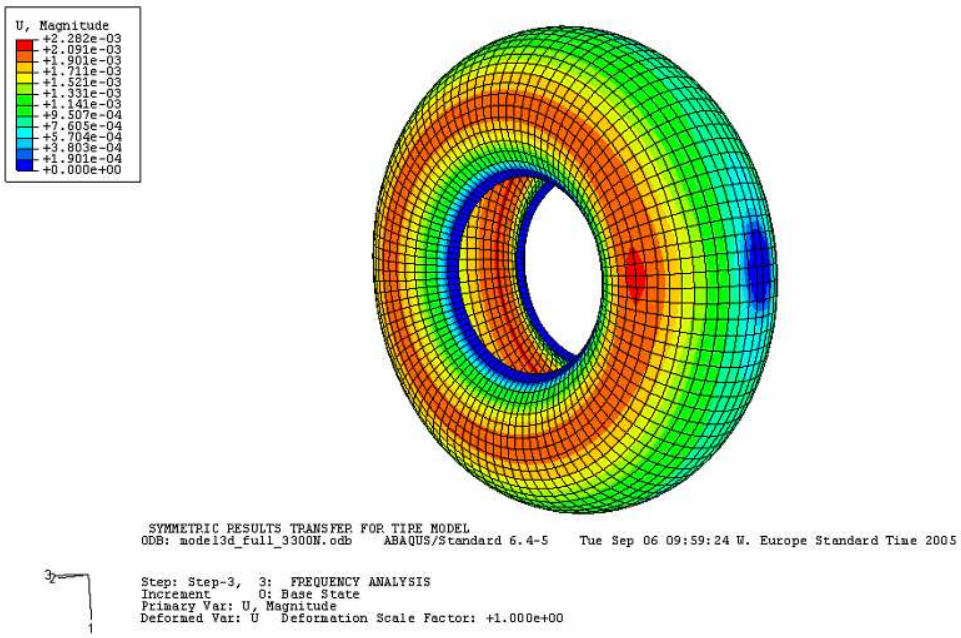

Figure 2.3: Simplified FE-model of the tire in a deformed stage.

2.1.3 Initial deformation

As said at the start of this section, the modal base is constructed around a non-rotating deformed tire model. Hence, the full non-linear tire model is used to describe this initial deformation. With this modal base, the vibrational response of the deformed tire due to road roughness deflecting the tire is determined. Thus the contact problem is divided into two parts. The development of the contact model to account for road roughness deflecting the tire is one of the aims of this research and is described in

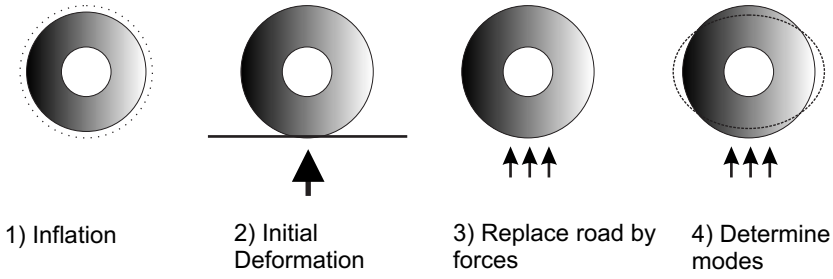

Figure 2.4: Initial tire deformation, the tire is first inflated whereafter the road is pressed against the tire and the contact forces are determined. After the forces are determined the road surface is replaced bij these forces and the eigenfrequencies and mode shapes of the deformed tire are determined.

chapter 5. Below only the initial deformation is considered and it is discussed how the modes at this deformed state are determined.

The tire is modelled in the FE package Abaqus. In Abaqus a flat road surface is pressed against the tire with an initial force. Blom [2005] has shown that there are differences between the situation where the modes are determined with the road surface pressed against the tire and with the road surface replaced by forces acting on the tire. If the road is not replaced by forces, the nodes in the contact patch are fixed to the road surface by Abaqus, which is not a realistic boundary condition. By replacing the road surface by forces this is avoided, see figure 2.4.

In Blom [2005] only vertical forces are used to initially deform the tire; therefore friction between the tire and road is not modelled (This means that the initial deformation, from which the modes are determined, is not fully correct). Since it is not straightforward to determine these friction forces another, more simple, solution is used. Here, the initial deformation is taken from a separate simulation including the road surface and friction (see figure 2.4 picture 2), but the eigenfrequencies and mode shapes are still determined with only the vertical forces. For the time being it is assumed that the influence of the friction forces on the determination of the modes can be neglected. The inclusion of these friction forces in the determination of the modes will be a subject of further research.

2.2 Method of working and structure of the tire/road model

In this section the build up of the tire/road model will be discussed. Figure 2.5 depicts the main functions of the tire/road model and how they correlate. As explained in the previous section, the first step is to determine the (non-linear) deformation of the tire due to a predefined load using a FE model of the tire. Then the eigenfrequencies and modeshapes of the pre-deformed tire are calculated. After the eigenfrequencies and mode shapes are determined, they are exported from the FE environment to the Matlab environment. To do this a separate script is used, which transforms an output file from Abaqus (of the format .fil) to an input file for Matlab (of the format .mat). This file contains the eigenfrequencies and mode shapes, the position of the tire nodes and information on how the tire model is built such as number of nodes and segments. With this information and a given rotational tire velocity, the system of equations, see (2.1) can be defined.

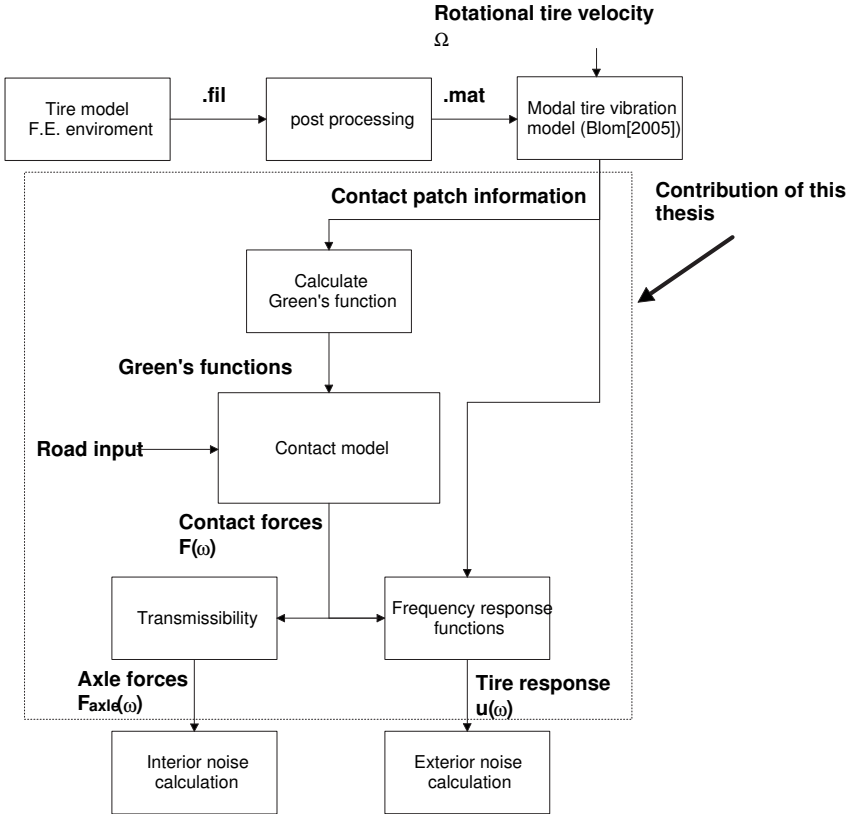

Figure 2.5: Build up of the tire/road model. The boxed area is the contribution of this thesis.

Now that the modal tire model is created, the contact problem can be solved. Note that in this modal tire model, a constant rotational velocity is used. To reduce the contact problem only a small part of the tire is considered, namely only the area near the contact patch (further called contact area). This is possible because the modal tire model is defined in the reference frame and consequently its mesh stands still (see the previous section). For the nodes of the contact area the Green's functions are determined, so that the dynamic response of the tire (the contact area) can be determined in the time domain. The reason of using Green's functions and how this is done will be explained in chapter 4.

Knowing the contact area and its Green's functions, the contact problem between the tire and the road roughness, which deflects the tire, can be solved. Hence a contact force history $F(t)$ for each contact point can be determined. Then the contact forces are Fourier transformed to the frequency domain, which enables the calculation of the total tire vibrations by multiplying the contact forces with the frequency response matrix, $\mathbf{u}(\omega) = \mathbf{H}(\omega)\mathbf{F}(\omega)$. Here the frequency response matrix $\mathbf{H}(\omega)$ is defined as (see de Kraker and van Campen [2000]):

$$\mathbf{H}_{nxn} = \mathbf{\Phi}[-\omega^2\tilde{\mathbf{M}} + i\omega\tilde{\mathbf{D}} + \tilde{\mathbf{K}}]^{-1}\mathbf{\Phi}^T \tag{2.9}$$

Also the axle forces, due to these contact forces in the frequency domain, can be determined using the transmissibility between contact area and wheel axle. These total tire vibrations and axle forces can then be used for exterior and interior noise calculations respectively.

Chapter 3

Literature study

In this chapter the literature study concerning contact models, for the use in a tire vibration model, is discussed. These contact models have to give the contact forces which act on the tire due to tire/road contact. The contact forces depend on the vibration of the tire itself, the road roughness and friction. Since the distribution of contact points changes constantly in time, the tire/road interaction is non-linear. Hence the contact problem has to be solved in the time domain. Because the aim of this research is to develop a contact model for the existing tire vibration model discussed in chapter 2, this literature study only concerns the contact models self.

3.1 Vertical contact models

When modelling the tire/road contact one of the first things that have to be taken into account are the vertical contact forces. The elastic foundation model, also called Winkler bedding, is generally used to calculate the vertical (or radial) contact forces. This Winkler bedding is a set of non-coupled, massless, linear springs which connect the two bodies to each other at the contact points. From the deformation of the springs the contact forces are calculated. Kropp [1999] and Burke and Olatunbosun [1997] use such a Winkler bedding. Main assumptions for this model are:

- Only when a point is in contact with the road a radial force can act there.
- The amplitude of this force depends on the local deformation of the tread at this point, i.e. a possible interaction with other points is not accounted for.

In Kropp [1999] the Winkler bedding represents the tire tread, where the springs are located at discrete points with stiffness s_e. The contact force F_e is then given by Hooke's law. Adhesive effects are neglected. Hence a force only acts at these points, when the springs are compressed. $F_e(N\Delta t)$ is thus given by:

$$F_e(N\Delta t) = s_e \Delta u_{z,e}(N\Delta t) H[-\Delta u_{z,e}(N\Delta t)] \tag{3.1}$$

with:

$$\Delta \mathbf{u}_z(N\Delta t) = \mathbf{u}_{z,0}(N\Delta t) + \mathbf{k}_{10}(N\Delta t) + \mathbf{u}(N\Delta t) - \mathbf{k}_2 \tag{3.2}$$

note that $\mathbf{k}_{10}(\phi, N\Delta t)$ and $\mathbf{k}_2(\phi)$ are defined in the negative y direction. The Heaviside function H is defined as:

$$H(x) = \begin{cases} 0, & (\text{x}<0) \\ 1, & (\text{x}\geq 0) \end{cases} \tag{3.3}$$

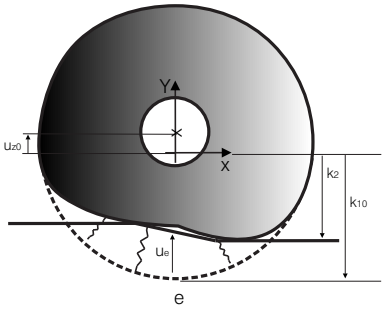

Figure 3.1: Representation of the Winkler bedding, for simplicity only three springs are drawn.

Here $\Delta u_{z,e}(N\Delta t)$ is the distance between point e on the tire and the road surface. $\Delta u_{z,e}(N\Delta t)$, as defined in (3.2), is a function of the displacement $u_{z,0}(N\Delta t)$ of the center of the rim, the position $k_{10}(\phi_e, N\Delta t)$ of point e when the belt is non-deformed, displacement $u_e(N\Delta t)$ of point e caused by the belt vibration and the roughness function $k_2(\phi_e)$ which describes the road. See figure 3.1. The belt vibration $u_e(t)$ is given by the convolution:

$$u_e(t) = \sum_m F_m(t) \otimes g_{m,e}(t) \tag{3.4}$$

where $g_{m,e}(t)$ is the Green's function representing the vibrational system with an input at the discrete point m and an output at the discrete point e. Because there is more than one contact force acting on the tire the response is calculated by superposition. Note that if there is no contact $\Delta u_{z,e}(N\Delta t)$ is larger than zero and the Heaviside function equals zero.

The main advantage of the Winkler bedding is its simplicity (especially when adhesion is neglected). However, the model consists of individual springs which neglects the interaction between the contact points. Hence the contact problem is not solved in a realistic manner. To include this interaction Kropp et al. [2003] use an elastic half-space as described in Johnson [1985]. The latter presents an overview of solutions for various contact problems. In particular, analytical solutions are available in order to relate the contact pressure and deflection of a three-dimensional elastic half-space. The pressure/deformation relationship used is derived by Love [1929] (see also Johnson [1985] chapter 3) and describes the effect of a uniform normal pressure acting on a rectangular area of size 2a x 2b in a (x,y,o) coordinate system, see figure 3.2. Note that the elastic half-space is semi-infinite and is not bounded by the rectangle A,B,C,D. A brief derivation of this relationship can be found in appendix E. Using this expression an influence matrix can be build which describes the pressure/deformation relationship for each point in the contact patch. In the latter the area 2a x 2b represents the contact area of one contact point. Hence an influence matrix is obtained which can describe the stiffness of the tire tread, including the cross correlations. To solve the contact problem an iterative algorithm is needed in order to determine what irregularity will actually be in contact with the elastic half-space and what deformation the elastic half-space will have. The relationship between pressure and deflection of the three-dimensional half-space at equilibrium is:

$$\Delta \mathbf{u}_z(t) = \mathbf{C}\mathbf{p}(t) \tag{3.5}$$

where $\Delta \mathbf{u}_z$ is the deformation vector, $\mathbf{p}$ the contact pressure vector and $\mathbf{C}$ the influence matrix built from the pressure relationship. $\Delta \mathbf{u}_z(t)$ and the contact force $\mathbf{f}(t)$ are calculated so that according to:

$$\mathbf{f}(t) = \mathbf{C}^{-1}\Delta \mathbf{u}_z(t)dxdy \tag{3.6}$$

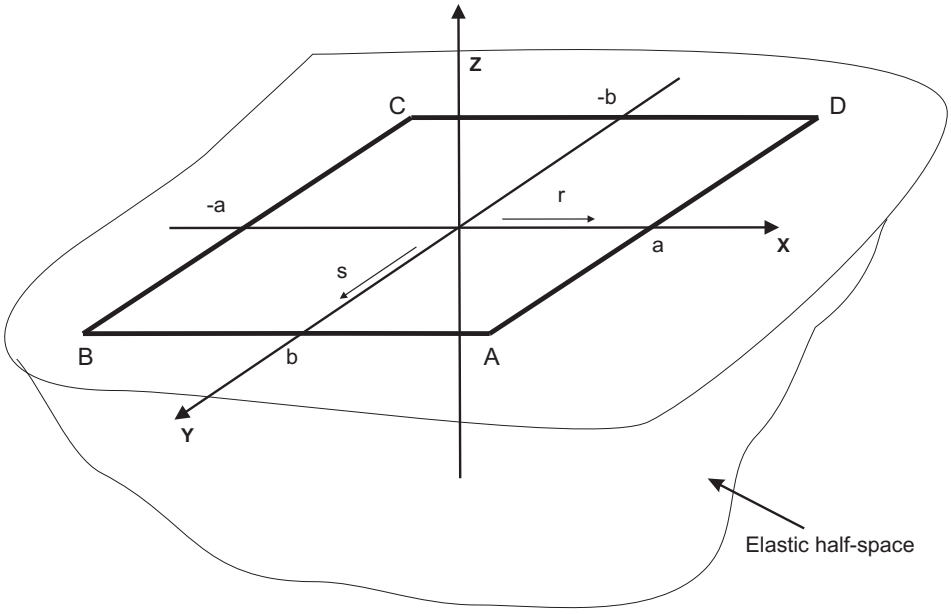

Figure 3.2: An elastic half-space

where dx and dy are the dimensions of a single area excitation. In order to find the correct $\mathbf{f}(t)$ and $\Delta\mathbf{u}_z(t)$ for each time step, an iterative algorithm is involved and written as:

$$\begin{cases} \mathbf{f}^{n+1}(t) = (\mathbf{C}^n)^{-1}\Delta\mathbf{u}_z(t)dxdy \\ \Delta\mathbf{u}_z^{n+1}(t) = \frac{\mathbf{C}\mathbf{f}^{n+1}(t)}{dxdy} \end{cases} \tag{3.7}$$

With $\Delta\mathbf{u}_z^0(t) = \mathbf{u}_{z,0}(t) + \mathbf{k}_{10}(t) + \mathbf{u}(t) - \mathbf{k}_2(t)$ (for the definition of these parameters see figure 3.1) and so that $\Delta\mathbf{u}_z^{n+1}(t) \geq \Delta\mathbf{u}_z^0(t)$. $\mathbf{C}^n$ is a sub-matrix of $\mathbf{C}$ for the points in contact at iteration n. The iteration stops if $\Delta\mathbf{u}_z^{n+1}(t) = \Delta\mathbf{u}_z^n(t)$ within a certain tolerance.

As with the Winkler bedding the contact problem has only to be solved in the contact patch, and the tire dynamics are included in the model. The main difference is the coupling between the contact points. Due to this coupling the contact model acts more like a real tire. A consequence of this coupling is that an iterative routine is necessary to determine the contact forces and displacements due to the road roughness. Also the elastic half-space is a semi-infinite medium that cannot describe the thickness of the tire tread or the effects of its finite width. Therefore the Young's modulus E has to be chosen in such a way that it compensates for those shortcomings.

Another way to include the coupling between the contact points is proposed by Larsson [2000]. In this work the tread blocks are directly included in the Green's functions. These Green's functions are transfer functions, in the time domain, which are used to calculate the tire response. In this way the coupling is taken into account since the transfer functions also describe the cross correlations between the points in the contact patch. Hereupon, since the tread blocks are modelled in the tire model, the problem of how to define the stiffness of the individual springs, as in a Winkler bedding, is avoided. To explain the working principle, figure 3.3 shows a vibrating structure in contact with a rough road surface. This structure is discretised in the space domain, so the contact forces and responses are only calculated at the discrete points. The response of the structure contact points is written as the

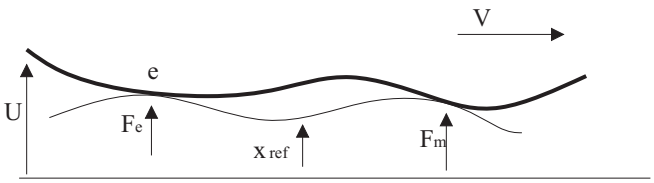

Figure 3.3: A structure, having profile u, in contact with a rough reference surface with profile x_{ref}. (Larsson and Kropp [2002]

convolution between the contact forces and Green's functions according to:

$$u_e(t) = \sum_m F_m(t) \otimes g_{m,e}(t) \tag{3.8}$$

where $g_{m,e}(t)$ is the Green's function representing the vibrational system with an input at the discrete point m and an output at the discrete point e. If there is more than one force, the response of the system can be calculated as the sum of the responses to each force. The transition to a time discrete representation gives:

$$u_e(N\Delta t) = \sum_m F_m(N\Delta t) g_{m,e}(0)\Delta t + \sum_m \sum_{n=0}^{N-1} F_m(n\Delta t) g_{m,e}[(N-n)\Delta t]\Delta t \tag{3.9}$$

The first part represents the displacements due to the current forces at time $N\Delta t$ and the second part corresponds to the displacements due to the forces working in the past. To find the solution, the following iterative method is used

- The displacement at time step $N\Delta t$, u_e^0, is first calculated assuming no contact. The response only depends on old forces, hence only the last part of (3.9) is used.
- If the surface of the structure penetrates the reference surface, a contact force will act opposite to the displacement. At the points in contact the following equation gives the necessary condition to be fulfilled.
$$\Delta u_e(N\Delta t) = x_{e,ref}(N\Delta t) - u_e^0(N\Delta t) \tag{3.10}$$
- The contact forces F_m, needed to create this displacement can be calculated by solving the linear system of equations given as:
$$\Delta u_e(N\Delta t) = \sum_m F_m(N\Delta t) g_{m,e}(0)\Delta t \tag{3.11}$$
Note that (3.11) holds for each point in contact.
- This iterative procedure is repeated for each time step.

Here $x_{e,ref}$ is the height of the reference surface and $u_e^0(N\Delta t)$ the displacement only dependent on the old forces. As with the elastic-half space used by Wullens and Kropp [2003] the coupling between points on the surface is taken into account. Also the problem of how to define the stiffness of the individual springs (Winkler bedding) is avoided. By modelling the tread blocks in the tire model the dynamics of these can be taken into account and the tread thickness and its finite width can be

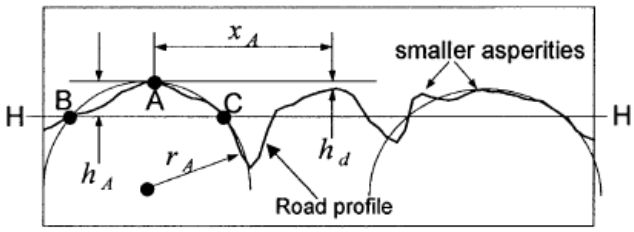

Figure 3.4: Road roughness parameters obtained from road profile and used with the contact model. (Fujikawa et al. [2005])

incorporated in this way. This is not possible in the elastic half-space. Nevertheless, the tread has to be included in the tire model. As a consequence the mesh of the FE model has to be finer which makes the vibration model slower. Fujikawa et al. [2005] avoid this inclusion of the tread, by using a totally different approach to calculate the vertical contact forces. Here the road is modelled using mean road roughness parameters and the tire is modelled as a constant shape, neglecting the tire response. The road roughness parameters are obtained from a measured road profile. Figure 3.4 depicts the road roughness parameters obtained from the measured road profiles. The profiles are separated by H-H representing a horizontal plane that divides the nominal contact area into two equal areas. Here, the parts above line H-H are treated as the asperities according to Fujikawa et al. [1994]. The road roughness parameters illustrated are then evaluated as follows: asperity height h_A is the height of the apex from line H-H. Asperity height unevenness h_d is the asperity height difference between the two nearest asperities. Asperity spacing x_A is the distance between adjacent asperities. Asperity radius r_A is the radius of the arc that includes three points in figure 3.4 A (apex of the asperity) B and C are the intersections between the profile and line H-H. The smaller asperities which are frequently contained in the arcs, as illustrated in figure 3.4, are neglected. After the road roughness parameters are determined the road is modelled as a sequence of spherical asperities. Hence Hertz formula of contact can be applied to calculate the contact forces at each point of the discretised tire surface. Assumptions that have been made are:

- The shape of the tire tread is uniform in the lateral direction.
- The tire is modelled in the contact region as a (flat) surface and the tire response is not taken into account.
- The effect of road roughness on tread vibration is approximately examined using uniformly distributed spherical asperities, with mean road roughness parameters.
- The tire travels with a constant velocity.

When the tire travels over the asperities, the contact between the tread and the asperities generates a vibratory contact force. This vibratory contact force is calculated as follows, first the forces of the higher and lower asperities are calculated. Secondly, these asperity forces are time shifted by t_A, as shown by the broken lines in figure 3.5, where $t_A = x_A/v$. Then, the shifted contact forces are summed as shown by the dotted line in figure 3.5. The oscillating component of the force is assumed to be the excitation force. This excitation force is then used to calculate the tire response. The model of Fujikawa et al. [2005] is created to investigate the detailed effects of road roughness parameters

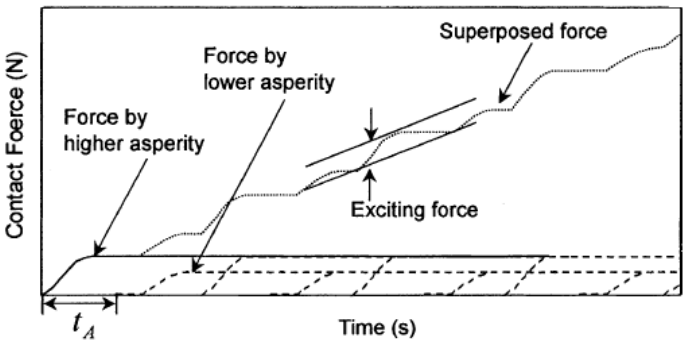

Figure 3.5: Exciting force obtained from the summation of the time shifted contact forces.(Fujikawa et al. [2005])

on tire tread vibrations. Therefore it models the road surface using mean road roughness parameters, incorporating the interaction between tire and road as indicated by Fujikawa et al. [1994]. Since mean road roughness parameters are used, and not the real road surface, not the real contact forces are calculated but only the vibratory contact force. To include the real road surface the previously discussed models have to be used or the models described in Mancosu and Minen [1998]. In the latter, two, vertical contact models are presented. The first model is currently implemented and the second is subject of on going development. The first contact model searches for tire road contact points and determines the penetration and velocity at those points. With this information and a subroutine, the impact forces at the contact points are determined. Unfortunately no detailed information of this vertical contact model or subroutine could be found. The second vertical contact model works on evaluating the intersecting volume of the tire and the road irregularities. To be able to detect the penetration between the tire and road irregularities, the tire is ideally divided into several wedges. The volume of these wedges can change at each iteration step as they are dependent on the static tire response. At every iteration the intersecting volume between the wedge and the three-dimensional road profile is computed. By means of a look up table derived from FE, the FE program Abaqus is used for this purpose, the resulting force at the contact nodes is calculated. The main advantage of these models is that they work with a real road surface and include the tire response, in contrast to Fujikawa et al. [2005]. However they do not incorporate the coupling between the contact nodes since the contact forces are determined for each wedge separately. Also the dynamic response of the tire is not included, in the second model, since the forces are calculated using only the intersection volume (between the wedge and road surface) and a look up table. For the first model there is not enough information to conclude something in this direction.

3.2 Horizontal contact models

Besides vertical forces also friction, or horizontal forces act on the tire. To calculate these horizontal ”contact” forces, a discrete Brush model is generally used. The model consists of individual elastic elements linked to the tire belt, see figure 3.6.

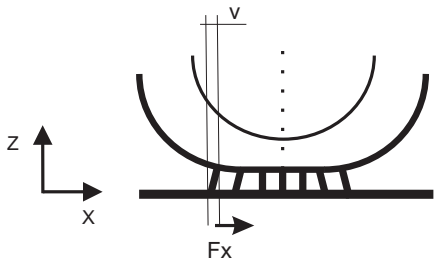

Figure 3.6: Discrete brush model.

To include the stick/slip behavior several states have to be determined, where it may be clear that without a normal force (vertical force) no friction forces can work. The different states can be defined as:

- No contact
$$F_x = F_y = 0 \tag{3.12}$$
- Contact and sticking
$$F_x^2 + F_y^2 \leq (\mu F_z)^2 \tag{3.13}$$
Where $F_x = K\,v$ and $F_y = K\,w$.
- Contact and slipping
$$F_x^2 + F_y^2 > (\mu_s F_z)^2 \tag{3.14}$$
where $F_x = \frac{v\mu F_z}{\sqrt{v^2+w^2}}$ and $F_y = \frac{w\mu F_z}{\sqrt{v^2+w^2}}$.

Here u, v, w are the displacements in the element co-ordinate system, K the value for the Brush stiffness, F the forces in x, y, z direction and μ the friction coefficient. In the above it is assumed that the tire tread can slip, as is also done in Burke and Olatunbosun [1997] where the Brush model is combined with a Winkler bedding to calculate the vertical contact forces. However, it can also be assumed that the tire tread does not slip. This is for example done in Mancosu and Minen [1998] where the values of horizontal slip, due to the roughness of the road, are assumed to be pretty small; therefore all brush elements in the contact patch adhere to the road surface. Hence only two states exist: no contact and contact.

3.3 Conclusion

During the literature study two sort of approaches are found. In the first approach the coupling between the contact points is neglected. This approach is for example used in Kropp [1999] and Burke and Olatunbosun [1997], where non-coupled springs are used to calculate the contact forces. This results in a simple contact model. In Mancosu and Minen [1998] (second model) the contact forces are calculated using separate wedges. Consequentially the coupling between the contact nodes, via the wedges, is neglected. The second approach includes the coupling between the contact points, see Wullens and Kropp [2004] and Larsson and Kropp [2002]. This coupling can be done in several ways. In Larsson and Kropp [2002] the tread is modelled within the tire model and uses the Green's

functions of the tire to determine the response and contact forces, thus coupling the contact points with the Green's functions of the system. In Wullens and Kropp [2004] an elastic-half space is used to couple the contact points. To model the horizontal "contact" forces a brush model is generally used, where the only difference lies in the assumption made if the tire can or cannot slip.

The literature study presented several contact models. However, not all contact models are suited for the purpose of this research. The Winkler bedding for example lacks the coupling between the contact nodes, which is desired to represent the contact problem fully. The contact model presented in Larsson and Kropp [2002] models the tread in the tire, which could be difficult in the tire model used and makes the FE model larger. The contact model presented by Fujikawa et al. [2005] uses mean road roughness parameters, so that the real nodal contact forces can not be determined. The work presented in Mancosu and Minen [1998] looks promising however detailed information is absent, so no real conclusion can be drawn.

To model the vertical contact forces the elastic half-space as presented in Wullens and Kropp [2004] is therefore considered the best model to be used. This model includes the coupling between the contact nodes using an elastic half-space. The forces are determined with an influence matrix. Since this matrix can be defined in advance of the contact simulation it is also computationally efficient. To model the horizontal contact forces a brush model will be used, since it can be well used with the elastic half-space. Tire slip will not be taken into account since the calculated deformation (when solving the contact problem), is additional to the initial deformation in FE, and considered to be small. Note also that the tire is steady-state rolling since Ω is constant. Hence it can be assumed that the tire does not slip under these conditions.

Summarizing, the contact model that will be implemented in the tire model during this thesis will consist of two parts. For the vertical forces the elastic-half space used in Wullens and Kropp [2004] will be implemented, and for the horizontal contact forces a brush model without slip will be used.

Chapter 4

Semi-analytical Green's functions

For modelling tire vibrations one is interested in the response of the tire due to contact forces originated from the tire/road contact. If one assumes that the distribution of contact points does not change in time, a frequency domain analysis can be performed to determine the frequency spectra of the contact forces. However when this assumption is dropped, this is not possible anymore since the tire/road interaction is then non-linear. Due to this non-linearity the contact problem has to be solved in the time domain. The response of the tire to the contact forces must therefore be obtained from the convolution product of the Green's functions and the contact forces. These Green's functions can be calculated by taking the inverse Fourier transform of the frequency response functions. In section 2.2 a definition of the frequency response matrix is given. So by taking the inverse Fourier transform of each of the elements of this frequency response matrix the Green's functions can be obtained. However, the tire model consists of a large number of dofs. Therefore calculating this frequency response matrix is computationally inefficient. Hence another solution is used, see Lopez et al. [2006]. Instead of taking the inverse Fourier transform of the frequency response functions a semi-analytical formulation of the Green's functions including rotation, has been derived. In this chapter it will be discussed how this formulation is created, where it has to be noted that there will only be worked in the reference frame.

4.1 Theory

The main idea is to decouple the set of equations (2.1) by solving the eigenvalue problem a second time (the first time is in Abaqus). Since the matrix $\tilde{\mathbf{D}}$ introduced in section 2.1.1 (2.3) can not be written as a linear combination of the mass and stiffness matrix, a general non-conservative system is obtained. In de Kraker and van Campen [2000] a method to decouple such a system is given. This method is briefly described below. For a full explanation of this method is referred to de Kraker and van Campen [2000], chapter 4. After the system equations are decoupled the Green's functions for the rotating tire can be derived easily.

In general the tire dynamic equations can be described by the following set of equations, where the total tire response is dependent of a force acting at point j, see figure 4.1:

$$\mathbf{M}_{nxn}\ddot{\mathbf{X}}_{nx1}(t) + \mathbf{D}_{nxn}\dot{\mathbf{X}}_{nx1}(t) + \mathbf{K}_{nxn}\mathbf{X}_{nx1}(t) = \mathbf{f}_{j,nx1}(t) \tag{4.1}$$

Here **M**, **D** and **K** are the mass, damping and stiffness matrices of the system and **f** a vector with the force working at point j. The subscript n stands for the number of dofs taken into account.

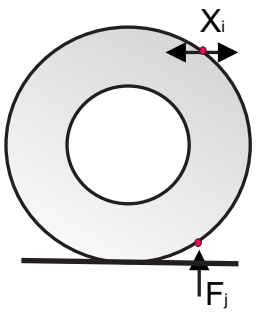

Figure 4.1: Definition of the actuating (j) and response (i) points on the tire.

The following transformation can be applied by solving the first eigenvalue problem and making the system mass normalized:

$$\mathbf{x}(t) = \mathbf{\Phi}\boldsymbol{\eta}(t) \tag{4.2}$$

Hence the dynamic equations of the system can be described in modal coordinates as:

$$\ddot{\boldsymbol{\eta}}(t) + \mathbf{D}_{mod}\dot{\boldsymbol{\eta}}(t) + \mathbf{K}_{mod}\boldsymbol{\eta}(t) = \mathbf{\Phi}^T_{j,mx1}F(t) \tag{4.3}$$

Note that this eigenvalue problem is solved in Abaqus. In (4.3) $\mathbf{K}_{mod}$ is a diagonal matrix with elements $k_{ii} = \omega_i^2$, where ω_i are the eigenfrequencies of the system. Since Raleigh damping is considered, $\mathbf{D}_{mod}$ is a diagonal matrix with elements $d_{ii} = 2\xi_i\omega_i$ where ξ_i are the modal damping ratios.

To obtain the dynamic equations of the rotating tire in a fixed reference system, the following transformation is applied:

$$\frac{D}{Dt} = \frac{\partial}{\partial t} + \Omega\frac{\partial}{\partial \beta} \tag{4.4}$$

where β is the angular coordinate in the fixed reference frame, see figure 2.1. Using (4.4) to transform (4.3), the dynamic equations of the rotating tire in a fixed reference frame can be obtained:

$$\ddot{\boldsymbol{\eta}}_{mx1}(t) + \tilde{\mathbf{D}}(\Omega)_{mxm}\dot{\boldsymbol{\eta}}_{mx1}(t) + \tilde{\mathbf{K}}(\Omega)_{mxm}\boldsymbol{\eta}_{mx1}(t) = \mathbf{\Phi}^T_{j,mx1}F(t) \tag{4.5}$$

The expressions for $\tilde{\mathbf{D}}$, $\tilde{\mathbf{K}}$ and $\tilde{\mathbf{M}}$ can be found in section 2.1.1. The subscript m stands for the number of modes taken into account.

To solve the second eigenvalue problem and to decouple the equations of motion de Kraker and van Campen [2000] propose to transform the system from second order to a first order system. Therefore a new vector is introduced:

$$\mathbf{y}(t) = \begin{bmatrix} \boldsymbol{\eta}(t) \\ \dot{\boldsymbol{\eta}}(t) \end{bmatrix}_{2mx1} \tag{4.6}$$

The system then becomes:

$$\mathbf{A}_{2mx2m}\dot{\boldsymbol{y}}_{2mx1}(t) + \mathbf{B}_{2mx2m}\mathbf{y}_{2mx1}(t) = \mathbf{r}_{2mx1}(t) \tag{4.7}$$

with for **A**, **B** and **r**(t):

$$\mathbf{A} = \begin{bmatrix} \tilde{\mathbf{D}} & \mathbf{I} \\ \mathbf{I} & \mathbf{0} \end{bmatrix}, \mathbf{B} = \begin{bmatrix} \tilde{\mathbf{K}} & \mathbf{0} \\ \mathbf{0} & \mathbf{-I} \end{bmatrix} and\ \mathbf{r}(t) = \begin{bmatrix} \mathbf{\Phi}_j^T F(t) \\ \mathbf{0} \end{bmatrix} \tag{4.8}$$

By determining the right and left eigenvalue of (4.7)

$$[s\mathbf{A}+\mathbf{B}]\,\mathbf{u}=\mathbf{0} \qquad [s\mathbf{A}+\mathbf{B}]^T\,\mathbf{w}=\mathbf{0} \tag{4.9}$$

the equations can be decoupled as shown below:

$$a_v\left[\dot{\delta}_q(t)-s_q\delta_q(t)\right]=\mathbf{w}^{q\,T}_{1xm}\mathbf{\Phi}^T_{j,mx1}F(t) \qquad q=1,2,...2m \tag{4.10}$$

with $\lceil a_q \rfloor = \mathbf{W}^T\mathbf{A}\mathbf{U}$ where $\mathbf{U}$ and $\mathbf{W}$ are matrices of eigenvectors from the right and the left eigenvalue problems respectively. $\delta_q(t)$ are the modal coordinates for the rotating tire, s_q the eigenvalues of the right eigenvalue problem, and $\mathbf{w}$ the top part of $\mathbf{W}$, as $\mathbf{W}$ is defined as:

$$\mathbf{W}=\begin{bmatrix}\mathbf{w}\\ \mathbf{w}\lceil s_q \rfloor\end{bmatrix}_{2mx2m} \tag{4.11}$$

This decoupled equation (4.10) is then transformed to the Laplace domain, where a transfer function can be defined as:

$$G_{qj}(s)=\frac{\delta_q(s)}{F(s)}=\frac{\mathbf{w}^{q\,T}_{1xm}\mathbf{\Phi}^T_{j,mx1}}{a_q}\frac{1}{s-s_q} \qquad q=1,2,...2m \tag{4.12}$$

Transforming this back to the time domain gives:

$$g_{qj}(t)=\frac{\mathbf{w}^{q\,T}_{1xm}\mathbf{\Phi}^T_{j,mx1}}{a_q}e^{s_q t} \qquad q=1,2,...2m \tag{4.13}$$

To set it back into cartesian coordinates, (4.13) is pre-multiplied by $\mathbf{\Phi}$ and $\mathbf{U}$, according to $y(t)=\mathbf{U}\delta(t)$ and $x(t)=\mathbf{\Phi}\eta(t)$. This leads to:

$$g_{ij}(t,\Omega)=\sum_k^m \Phi_i^k\left[\sum_q^{2m} U_k^q\frac{\sum_p^m w_p^q\Phi_j^p}{a_q}e^{s_q t}\right] \tag{4.14}$$

4.14 is the Green's function for a force on point j to a displacement at point i, see figure 4.1. Note that $x_i(t)=\mathbf{\Phi}_i\boldsymbol{\eta}(t)$. Also note that only the top half of $\mathbf{U}$ is used since the subscript k goes until m whereas the matrix $\mathbf{U}$ has size $2mx2m$.

The Ω dependency of g_{ij} has been explicitly included in (4.14) to stress the fact the Green's functions are determined in the fixed reference frame and will change if the rotational velocity changes. It is also important to note that the only data needed for (4.14) are the eigenvalues and eigenvectors of the tire in the tire reference frame, which can readily be obtained from a FE model of the tire, and the mass matrix from the FE model. The Green's functions defined in (4.14) can be substituted in (4.15) to calculate the response of the rotating tire in a fixed reference frame.

$$\mathbf{x}_{nx1}(t,\Omega)=\begin{bmatrix} g_{1,1}(t,\Omega) & .. & g_{1,j}(t,\Omega) & .. & g_{1,n}(t,\Omega)\\ .. & & & & ..\\ g_{i,1}(t,\Omega) & .. & g_{i,j}(t,\Omega) & .. & g_{i,n}(t,\Omega)\\ .. & & & & ..\\ g_{n,1}(t,\Omega) & .. & g_{n,j}(t,\Omega) & .. & g_{n,n}(t,\Omega)\end{bmatrix}_{nxn}\otimes\mathbf{f}_{nx1}(t) \tag{4.15}$$

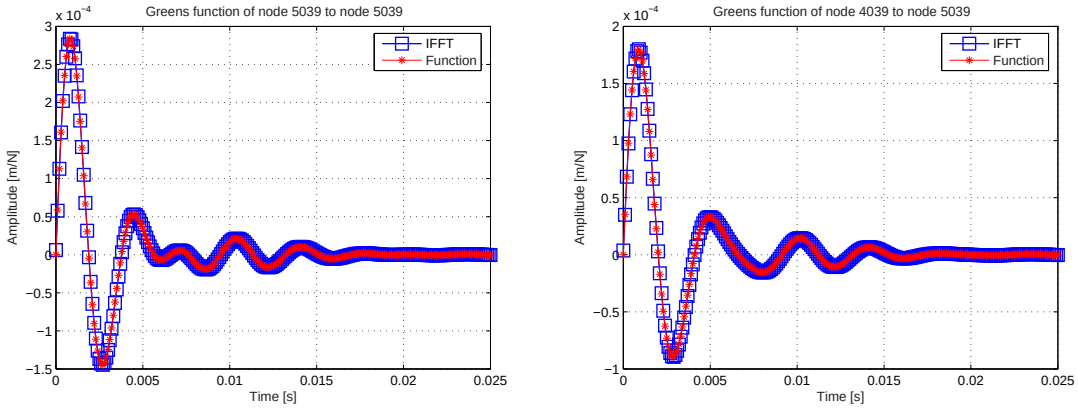

Figure 4.2: Green's function of the non-rotating tire using 10 modes and γ_1=500 (γ_2 = 0) Ns/(mkg). The plotted Green's functions are for the actuated (j=i) and neighbor (j≠ i) node respectively.

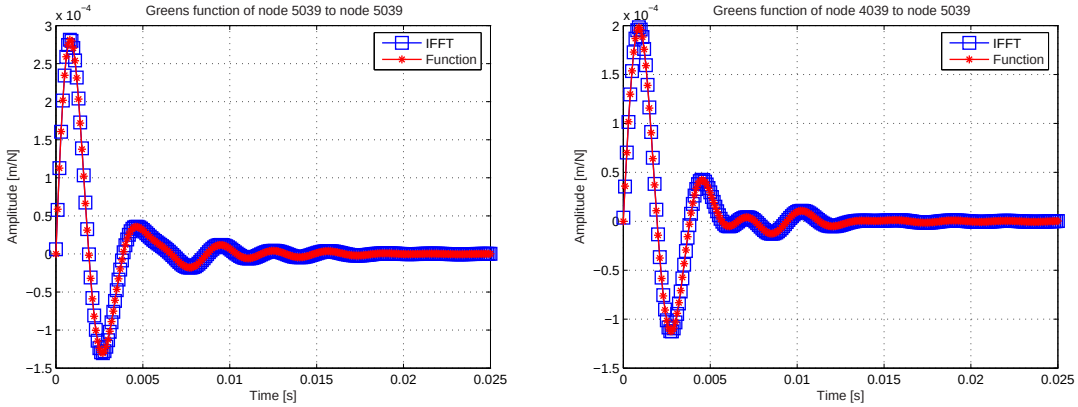

Figure 4.3: Green's function of the rotating tire at Ω=100 rad/sec, using 10 modes and γ_1=500 (γ_2 = 0) Ns/(mkg). The plotted Green's functions are for the actuated (j=i) and neighbor (j≠ i) node respectively.

4.2 Validation

To validate if this approach can be used, it is compared with the Green's functions obtained by using an inverse Fourier transformation of the frequency response matrix. Using the modes and eigenvalues determined in the eigenvalue analysis in Abaqus, the frequency response matrix can be defined as (see de Kraker and van Campen [2000]):

$$\mathbf{H}_{nxn} = \mathbf{\Phi}[-\omega^2\tilde{\mathbf{M}} + i\omega\tilde{\mathbf{D}} + \tilde{\mathbf{K}}]^{-1}\mathbf{\Phi}^T \tag{4.16}$$

Where $\tilde{\mathbf{M}}$, $\tilde{\mathbf{D}}$ and $\tilde{\mathbf{K}}$ are defined as in (2.2),(2.3) and (2.5). Figure 4.2 and 4.3 display the results obtained from the inverse Fourier transformation and the results from (4.14), for a non-rotating and rotating tire. It can be seen that the results obtained with the two approaches agree.

4.3 Results

In the previous sections it is shown how the semi-analytical expression for the Green's functions is derived. Also some validation of the approach is performed. However, the unique quality of the tire model, incorporating rotation, is not discussed. To show the effect of rotation on the Green's functions, this section will briefly present some of the results obtained with this approach. The tire model used for these results is the same as is discussed in chapter 2.1.2.

Blom [2005] has shown that a non-deformed, non-rotating tire has double eigenfrequencies with the same mode pattern but rotated $\frac{180}{2n_k}$ degrees where n_k is the number of waves along the circumference. When a tire rotates these eigenfrequencies shift leading to a split in eigenfrequencies. As shown by Kim and Bolton [2001], in the case of a non-deformed tire, the eigenfrequencies will shift $\pm(n_k \frac{\Omega}{2\pi})$ Hz, where Ω is the rotational velocity. This splitting can also be seen when the eigenfrequencies are determined from the rotating tire using the methodology presented in this chapter, where the eigenfrequencies equal $imag(s_r)/2\pi$. The result is shown in figure 4.4, where the eigenfrequencies of the first 10 modes are plotted.

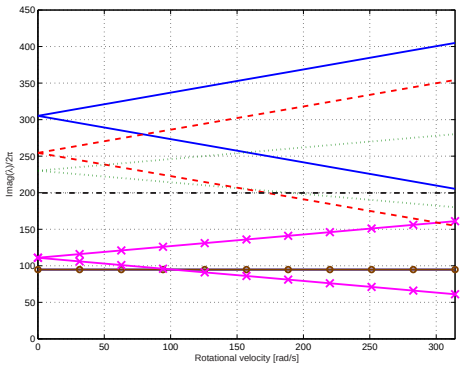

Figure 4.4: Eigenvalues of the first 10 modes for different Ω's

To show the effect of rotation on the Green's functions, two Green's function are calculated with different values for the rotational velocity: Ω = 0 and 100 rad/s. In these calculations the first 50 modes and a damping factor $\gamma_1 = 100$ Ns/(mkg) are used. Figure 4.5 (left) shows the results. In the right figure the corresponding admittance, obtained from an FFT of the Green's functions is shown. From the figures it can be concluded that there is a considerable difference in frequency and amplitude for rotational speeds of 0 and 100 rad/sec. The reason for the decrease in amplitude can be found in the increase of damping due to rotation, see (2.3). From figure 4.5 (right) it can be concluded that the frequency shift due to rotation is correctly predicted.

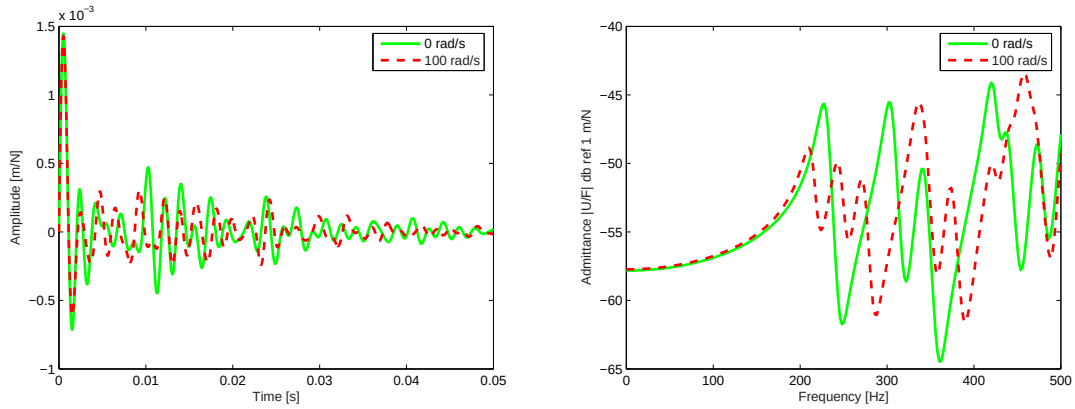

Figure 4.5: Response calculated using 50 modes and $\gamma_1 = 100$ ($\gamma_2 = 0$) Ns/(mkg), for $\Omega = 0$ and 100 rad/s. The right figure displays the Green's functions and the left figure the admittance.

4.4 Conclusions

To calculate the dynamic time response of the tire due to the contact forces, a convolution between the Green's functions and contact forces must be performed. In this chapter a semi-analytical expression for these Green's functions is created. This is done by decoupling the set of equations (2.1) by solving the eigenvalue problem a second time. From these decoupled equations the Green's functions are determined. Since the modal damping matrix of the rotating tire cannot be described as a linear combination of the mass and stiffness matrix, two eigenvalue problems are solved (the right and left eigenvalue problem).

Finally, comparing the results of this semi-analytical expression with the inverse fourier transform of the frequency response functions, it is demonstrated that the expression is correct. Also the effect of rotation is discussed where it is shown that the eigenvalue shift due to rotation is predicted correctly.

Chapter 5

Contact modelling

In this research the aim is to create a model which can calculate the tire vibrations of a tire rolling on a rough road surface. Hence the complex contact problem, between the tire and road, has to be solved. From the literature study it has been concluded that an elastic half-space (as used in Wullens and Kropp [2004]) in combination with a brush model is considered to be most suitable, to determine the contact forces between tire and road. In this chapter first the use of a contact model will be discussed. Hereafter the tire response, contact models and how the contact problem is solved will be discussed.

5.1 Contact modelling used in this research

The tire model used in this research is a rubber torus modelled in the finite element program Abaqus. By initially pressing the road surface against the tire in Abaqus, the tire is pre-deformed. In this way, the non-linear effects of the initially large tire deformation are incorporated. From this deformed tire the eigenfrequencies, mode shapes and mass matrix are determined as discussed in chapter 2. This data is given as input to the tire vibration model to be able to calculate the response from contact forces working on the tire. Hence the tire is largely deformed in the FE environment and has only small additional deformations in Matlab, which are assumed to be linear. Therefore the contact model is only used to determine the additional, and variational, contact forces working on the tire due to the road roughness,

$$F = F_{FE} + \tilde{F} \tag{5.1}$$

Here F_{FE} represents the constant forces obtained from the FE environment and $\tilde{F}$ the additional varying contact forces calculated in Matlab. The latter are responsible for the vibrational response of the tire. For notational convenience the tilde on $\tilde{F}$ will be omitted from now on. Once the contact problem is solved, the contact forces can be used to calculate the total tire vibration.

Modelling the tire in FE, one can question what the contact model physically represents. Here the contact model represents the tire tread in the contact patch. Hence it forms an additional layer around the tire which represents the stiffness of the tread. For the contact problem the assumptions where made that only when a point is in contact with the road surface a force can act. In addition the tire does not adhere to the road surface; so only positive vertical forces can act in the contact patch. To solve the contact problem the following routine is used, as is shown in figure 5.1.

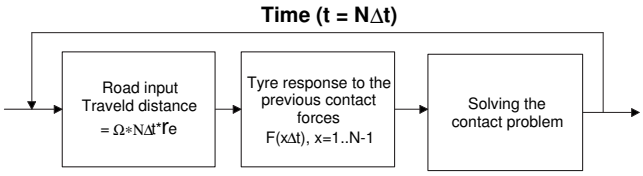

Figure 5.1: Overview of the implementation of the contact model.

- First, the road profile is taken. Since the tire is assumed to roll over a road surface with a constant velocity Ω, the road profile in the contact patch changes each time step. The displacement of the wheel center can be obtained as: $\Omega N \Delta t r_e$
- Secondly the response of the tire is calculated using only the previous contact forces ($\mathbf{f}(x\Delta t)\ with\ x = 0..N-1$) coming from the past. This calculation is left outside the solving routine for the contact problem, because it is not necessary to recalculate this response within one time step, since these forces do not change. Therefore this response can be seen as a constant when solving the contact problem.
- Hereafter the contact problem is solved as an initial value problem. Note that the tire response is the response due to the actual contact forces ($t = N\Delta t$) summed with the response due to the previous contact forces.
- This is repeated for each time step N.

The vertical contact model that will be used is the elastic half-space which will be implemented as is displayed in figure 5.2. The elastic half-space, which is in reality semi-infinite, will be bounded by a region near the contact patch. In the figure this is the area A,B,C,D. This contact region is kept some what larger than the contact patch itself so that the contact patch can become larger or change a bit. The area 2ax2b is the nodal contact area on which the individual contact forces act (this small rectangular area represents one peak in the road surface texture). Remember that outside the contact patch no contact forces exist. In section 5.3 the elastic half-space will be discussed in more detail.

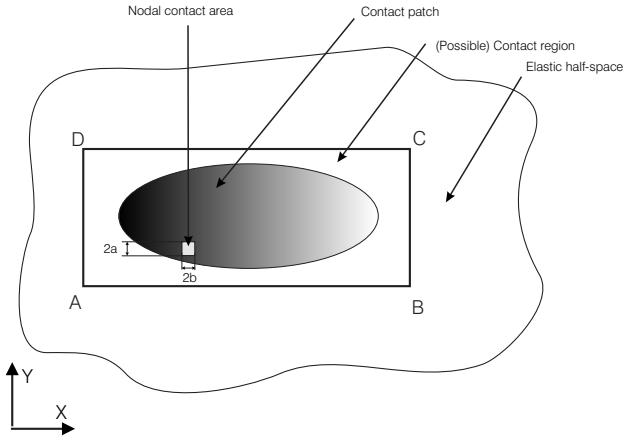

Figure 5.2: Elastic half-space implementation, note that the contact region is larger than the contact patch.

5.2 Tire response

As indicated in chapter 4, when modelling the tire vibrations one is interested in the response of the tire to contact forces originated from the tire/road interface. If one assumes that the distribution of contact points does not change in time, a frequency domain analysis can be performed to determine the frequency spectra of the contact forces. However, when this assumption is dropped, since the distribution of contact points does change constantly in time, this is not possible anymore since the tire/road interaction is then non-linear. Due to this non-linearity the contact problem has to be solved in the time domain. Therefore the response of the tire to the contact forces must be obtained from the convolution product of the Green's functions and the contact forces.

$$u_i(t) = \sum_j F_j(t) \otimes g_{j,i}(t) \tag{5.2}$$

Here F_j is the contact force at point j and u_i the response at point i on the contact patch. $g_{j,i}(t)$ is the Green's function representing the vibrational system of the tire, with an input at the discrete point j and an output at the discrete point i. Because there is more than one contact force acting on the tire, the response of the system is calculated by superposition. Transforming (5.2) (for $T = 0..N\Delta t$) into a time discrete representation, with time interval $N\Delta t$, leads to

$$u_i(N\Delta t) = \sum_j F_j(N\Delta t) g_{j,i}(0)\Delta t + \sum_j \sum_{n=0}^{N-1} F_j(n\Delta t) g_{j,i}[(N-n)\Delta t]\Delta t \tag{5.3}$$

5.3 The vertical contact model

From the literature study it became clear that using the elastic half-space, as a contact model to predict contact forces working between road and tire, is an attractive option. Hence some understanding of the elastic half-space is required. Therefore this section will shortly discuss the elastic half-space and its implementation.

5.3.1 The elastic half-space

An elastic half-space is a plane surface bounding different bodies, by considering each body as a semi-infinite elastic solid. This can be motivated in the following way, C.F. Johnson [1985].

"Non-conforming elastic bodies in contact whose deformation is sufficiently small for the linear small strain theory of elasticity to be applicable inventively make contact over an area whose dimensions are small compared with the radii of curvature of the undeformed surfaces. The contact stresses are highly concentrated close to the contact region and decrease rapidly with distance from the point of contact. Hence the area of interest lies close to the contact. Thus, provided the dimensions of the bodies themself are large compared with the dimensions of the contact region, the stresses in this region are not critically dependent upon the shape of the bodies distant from the contact area. The stresses may then be calculated to good approximation by considering each body as a semi-infinite elastic solid bounded by a plane surface i.e. an elastic half-space. This idealization, in which bodies of arbitrary surface profiles are regarded as semi-infinite in extent and having a plane surface, is made almost universally in elastic contact stress theory. It simplifies the boundary conditions and makes available the large body of elasticity theory which has been developed for the elastic half space". If there are different forces acting on the elastic half-space the total displacement can be found with superposition.

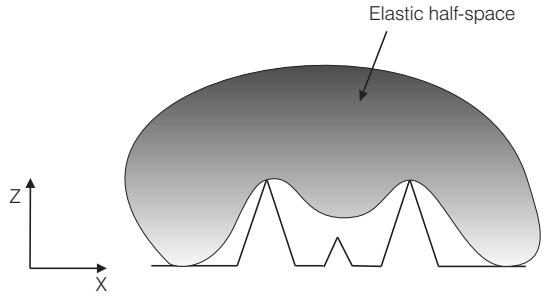

Figure 5.3: Elastic half-space deflecting by roughness peaks, note that the middle peak is not in contact.

5.3.2 Implementation

The elastic half-space is used to represent the stiffness of the tire tread, where the big advantage of the elastic half-space is the coupling between the contact nodes. To give a small impression of what is meant with this coupling, figure 5.3 depicts an elastic half-space deflected by three peaks. It can be seen that not only the forced point is deflected but also the adjoining points. In reality this is exactly what happens if a tire is deflected by a roughness peak/profile.

Several force/displacement relations are available for an elastic half-space, however in this research the work of Kropp [1999] will be followed. Therefore the following equation is used, which calculates the displacement Δu_z at position xy from the nodal contact area $2ax2b$ on which a uniform pressure p acts.

$$\begin{aligned}\frac{\pi E}{1-v^2}\frac{\Delta u_z}{p} = & \\ & + (x+a)ln\frac{(y+b)+\sqrt{(y+b)^2+(x+a)^2}}{(y-b)+\sqrt{(y-b)^2+(x+a)^2}} \\ & + (y+b)ln\frac{(x+a)+\sqrt{(y+b)^2+(x+a)^2}}{(x-a)+\sqrt{(y+b)^2+(x-a)^2}} \\ & + (x+a)ln\frac{(y-b)+\sqrt{(y-b)^2+(x-a)^2}}{(y+b)+\sqrt{(y+b)^2+(x-a)^2}} \\ & + (y-b)ln\frac{(x-a)+\sqrt{(y-b)^2+(x-a)^2}}{(x+a)+\sqrt{(y-b)^2+(x+a)^2}}\end{aligned} \tag{5.4}$$

here E and v are the Youngs modulus and the Possoin ratio of the elastic half-space. With equation 5.4 an influence matrix $\mathbf{C}$, valid for the total contact area, can be defined. This matrix represents the stiffness of the tire tread for all contact nodes, including the cross correlation (coupling) between the contact nodes. Hence matrix $\mathbf{C}$ is a square matrix of size nxn where n is the number of nodes in the contact region. With $\mathbf{C}$ the contact forces can be determined according to:

$$\Delta\mathbf{f}(t) = \mathbf{C}^{-1}\Delta\mathbf{u}_z(t)dxdy \tag{5.5}$$

The multiplication with $dxdy$ is to calculate the contact forces from the contact pressure. $\Delta\mathbf{u}_z$ is the deformation vector of the elastic half-space in vertical direction. The derivation of (5.4) can be found in appendix E.

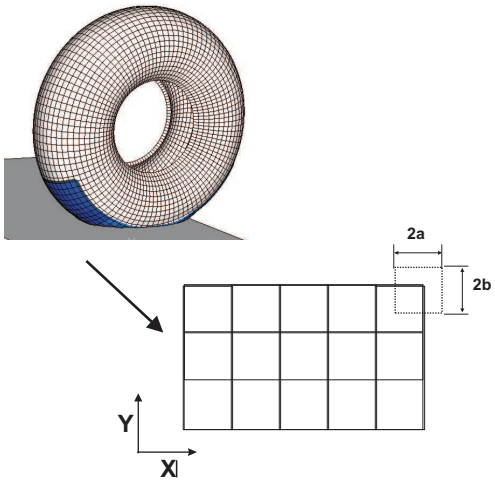

Figure 5.4: Visualization of a small peace off contact region which is divided in equal nodal contact areas. Note that $\Delta x = 2a$ and $\Delta y = 2b$.

It may be clear that for implementing the elastic half-space some parameters have to be defined. Figure 5.4 depicts some of these parameters. Here a and b are the width and length of the nodal contact area (dotted line) on which the pressure acts. a and b are calculated with the assumption that all the nodes are situated at the same distance from each other, as in a uniform grid. To calculate a and b, the coordinates of the begin node and end node of the contact patch are determined and the distance between them is divided in equal spaces. As is discussed by Wullens and Kropp [2004] the elastic half-space is a semi-infinite medium which cannot describe the thickness of the tire tread or the effects of its finite width. Consequently the Young's modulus E has to be chosen such that it compensates for those shortcomings. This will be done with the use of some static Abaqus simulations. Assumptions that are made:

- The area on which the pressure acts is for all the nodes of the same size, $2a \times 2b$.
- Only positive forces can act on the contact patch. If a contact force becomes negative its value is set to zero, hence adhesion is neglected. This is checked every iteration step of the solving routine.

5.3.3 Comparison with the literature

To check if the elastic half-space is correctly used, a simulation is made and compared with the results shown in Wullens and Kropp [2004]. The simulation consists of an elastic half-space deflected by some roughness peaks, see figure 5.5. In the literature study the structure of the iteration routine can be found,which is the same as discussed here. The results show a good agreement with those presented by Wullens and Kropp [2004]. Therefore, the implementation of the elastic half-space is correct. Figure 5.5 also shows the correlation between the nodes as a force acts at only one node. Instead of a sharp peak that would occur if the nodes where not coupled, the adjoining nodes are also displaced. This is more likely to occur in a real situation.

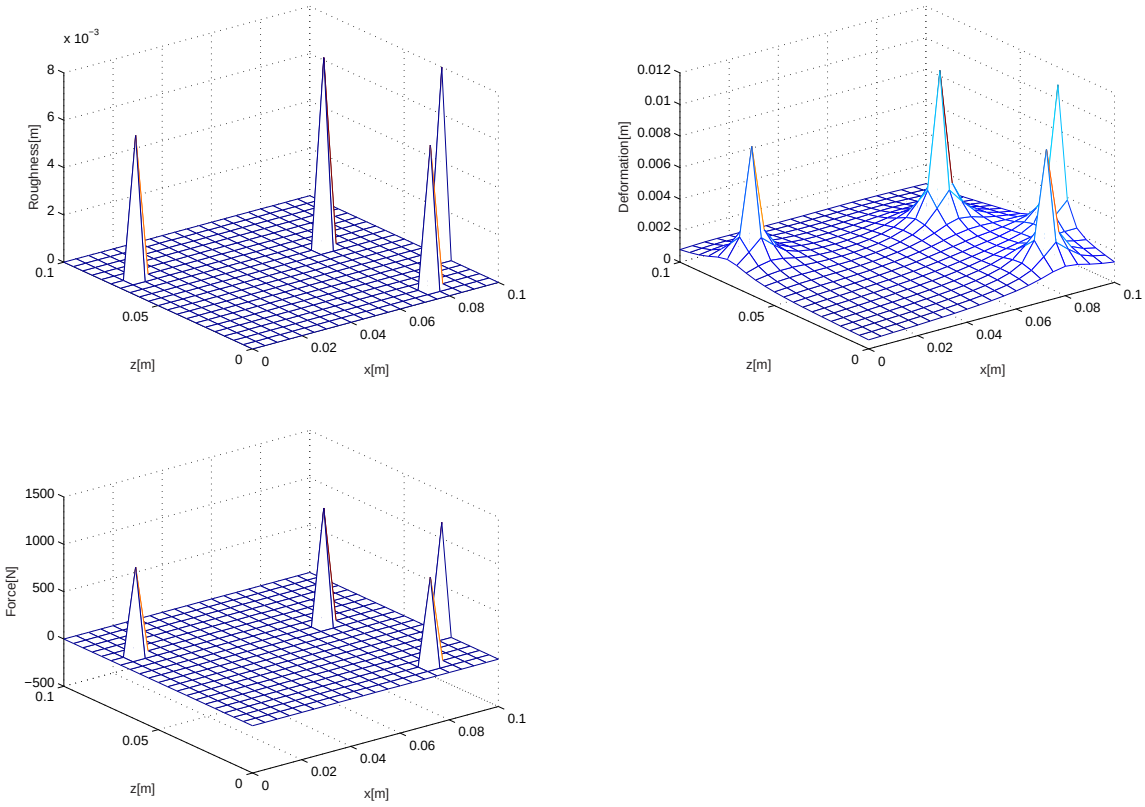

Figure 5.5: Results of the deformed elastic half-space, with $E = 20MPa$ *and* $v = 0.49$.

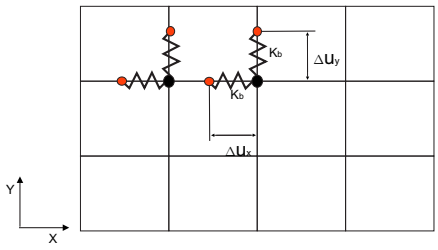

Figure 5.6: Overview of the contact region where two brushes are shown. Note that the springs are not coupled and have no initial length.

5.4 The horizontal contact model

As may be clear frictional forces act in the horizontal plane. To model these forces a brush model is used. It is assumed that the deformations are small, since the tire is steady-state rolling (Ω is constant in the determination of the Green's functions). Hence no sliding will occur. Therefore the brush model only consists of a stiffness (a spring) to represent the nodal force/deformation relationship as:

$$F_x = -K_b \Delta u_x \qquad F_y = -K_b \Delta u_y \tag{5.6}$$

Here K_b is the tire tread horizontal stiffness which is assumed to be the same for the x and y direction. The length of the springs is initially zero, and the forces are only dependent on the displacement of the brush elements, which is the same as the deformation calculated in Matlab. Note that there is no-coupling between the contact nodes or a coupling between F_x and F_y. Since frictional forces only act when a vertical force is present, only at points where there is a vertical force the frictional forces are calculated. Figure 5.6 displays the physical interpretation of the horizontal contact model.

5.5 Road input

Due to the tire rotation the road surface in the contact patch changes each time step. In the modelling approach used in this thesis the tire mesh stands still. Therefore not the tire moves but the road surface. How much the road surface moves is calculated with:

$$shift = \Omega \Delta t N r_e \tag{5.7}$$

where Ω is the tire rotational velocity, Δt the time interval between the time steps, N the current time step and r_e the effective rolling radius. Since the tire deformation is small (only small road roughness is considered) the effective rolling radius can be seen as a constant value.

Since the contact models used in this research are all discrete models the road surface also has to be discrete. Upon this, the coordinates of the tire contact nodes continually change due to tire vibration and rotation. Therefore in the solving routine of the contact problem, the road surface is discretised to the current contact point coordinates. To do this, a two dimensional linear interpolation routine is used. Figure 5.7 displays the tire and road where it can be clearly seen that interpolation between the road points is necessary to determine the road roughness at the contact nodes.

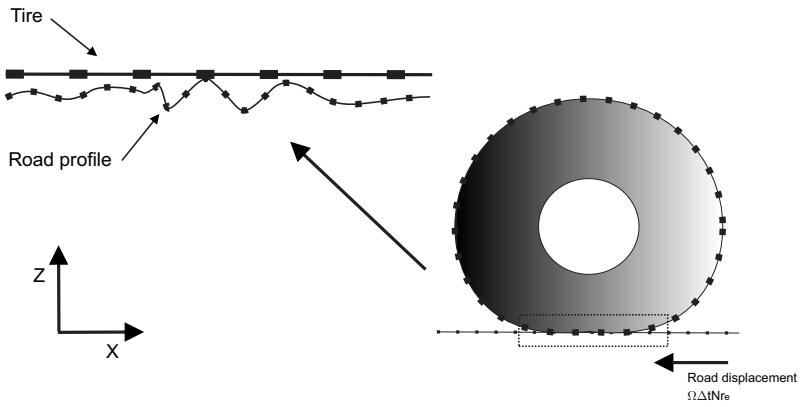

Figure 5.7: Overview of the discrete tire and road profile. Note that the road points do not have the same x coordinate as the tire nodes, making interpolation necessary.

5.6 Solving the contact problem

To solve the contact problem, it will be treated as an initial value problem which will be solved for each time step. Hence a function has to be defined which will be solved at each of these time steps. In the following this function will be derived.

From figure 5.8 the following formula can be defined:

$$\Delta \mathbf{u}_z = -1 * \{(\mathbf{z}_{begin} + \mathbf{u}_{response,z} + \mathbf{u}_{initialdeformation,z}) - \mathbf{z}_{road}\} \tag{5.8}$$

where $\Delta \mathbf{u}_z$ is the penetration of the tire by the road. A positive $\Delta \mathbf{u}_z$ means that there is contact between road and tire. Note that z are absoluut coordinates and u are relative coordinates. The tire response is calculated with:

$$\mathbf{u}_{response} = \mathbf{f} \otimes \mathbf{G} \tag{5.9}$$

and for the contact forces.

$$\begin{aligned} \mathbf{f}_x &= -K_b \Delta \mathbf{u}_x \\ \mathbf{f}_y &= -K_b \Delta \mathbf{u}_y \\ \mathbf{f}_z &= \mathbf{C}^{-1} \Delta \mathbf{u}_z dx dy \end{aligned} \tag{5.10}$$

Here K_b is the brush stiffness, $\Delta \mathbf{u}_{x,y}$ the displacement of the brush elements and $\mathbf{G}$ a matrix containing the Green's functions, see (4.15). The vector $\mathbf{f}$ contains the contact forces and $\mathbf{C}$ is the influence matrix built from (5.5).

Substituting (5.9) into (5.8), and using the condition that the tire does not slip (the displacement of the brush elements must be the same as the tire response) the initial value problem becomes:

$$\begin{aligned} \mathbf{\Pi}(\Delta \mathbf{u}_x) &= \mathbf{u}_{response,x} - \Delta \mathbf{u}_x \\ \mathbf{\Pi}(\Delta \mathbf{u}_y) &= \mathbf{u}_{response,y} - \Delta \mathbf{u}_y \\ \mathbf{\Pi}(\Delta \mathbf{u}_z) &= -1 * (\mathbf{z}_{begin} + \{\mathbf{f} \otimes \mathbf{G}\} + \mathbf{u}_{initialdeformation,z} - \mathbf{z}_{road}) - \Delta \mathbf{u}_z \end{aligned} \tag{5.11}$$

Here $\mathbf{\Pi}$ is a vector containing the initial value problem, which has to become zero ($\Pi(\Delta \mathbf{u}) = 0$). To solve this initial value problem the standard optimization toolbox of Matlab is used. As initial value

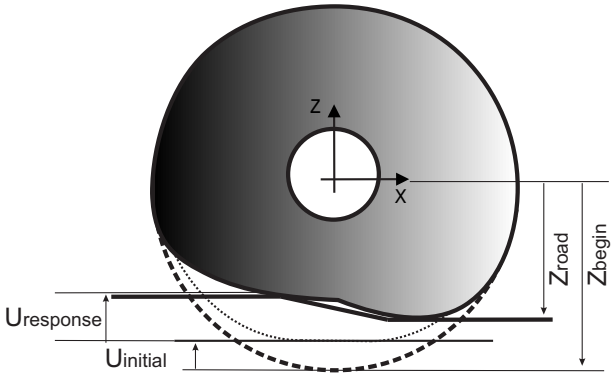

Figure 5.8: Tire coordinates.

for $\Delta\mathbf{u}_z$, (5.8) is used with for $\mathbf{u}_{response} = \mathbf{u}_{response}((N-1)\Delta t)$. The initial value taken for $\Delta\mathbf{u}_x$ and $\Delta\mathbf{u}_y$ is zero.

Since the response has to be calculated after the forces are determined and since the horizontal forces are a function of the response, the first iteration (at t=0) of the initial value problem cannot include horizontal forces. As a consequence the problem may become unstable and will not give the correct answer. To solve this, numerical damping is introduced. When the calculated horizontal forces (F_x and F_y) are much larger than the horizontal forces of the previous iteration the calculated forces are reduced. This is implemented as follows:

$$\begin{aligned} F_x &= F_x - \xi|F_x - F_{old,x}| \\ F_y &= F_y - \xi|F_y - F_{old,y}| \end{aligned} \tag{5.12}$$

Here ξ is a damping factor. Hence a stable problem is obtained and the problem is solved correctly.

5.7 Summary

In this chapter the manner on which the contact is modelled is discussed, starting with the initial deformation in Abaqus which leads to a split in contact forces. Hereafter the calculation of the tire response is discussed, where the tire response is divided into two parts: the response to the previous contact forces and the response to the current contact forces. To calculate the vertical contact forces the elastic half-space is used. Some comparison with literature is made to check if the elastic half-space is used correctly. It is shown that the results are in good agreement. To model the horizontal forces a brush model without slip is implemented, since the deformations are assumed to be small. The road surface is discretised using a two dimensional interpolation, so that the road surface height is known at the coordinates of the contact nodes. To solve the contact problem it is treated as an initial value problem which is solved for each time step in the simulation. For the first iteration (at t=0) the initial value problem can become unstable. To cope with this numerical damping is introduced.

Chapter 6

Validation with Abaqus

In this chapter the tire model and contact model of the previous chapters will be validated with the finite element package Abaqus. However, before an actual comparison will be made, first some attention will be given to the validation model itself.

6.1 Validation model

6.1.1 Use of Abaqus to validate

To validate the created model the finite element package Abaqus is used. As explained in chapter 2, the non-linear tire deformation due to a prescribed load is modelled in Abaqus. The eigenfrequencies and mode shapes are determined in Abaqus as well. Therefore, it seems a natural choice to use Abaqus results as a reference for comparison. In the methodology described in chapter 2, the rotation of the tire is included by applying a transformation from the tire coordinate system to a fixed reference system. Hence the tire mesh stands still, and not the total tire mesh has to be taken into account when solving the contact problem. In Abaqus this cannot be done, and the total, rotating, tire mesh has to be used. The results of Abaqus can then be transformed to obtain the response in the contact patch. However, this is computationally very expensive. Therefore the simulations in this chapter will be done with a non-rotating tire. However, no error due to rotation is expected since the tire response displays all the correct effects when rotation is applied, like the Doppler shift.

6.1.2 The simplified tire model

Until so far the tire model discussed in chapter 2 is used to create the modal base for the model. However only a relatively little number of modes is used. Hence the response shows the right influences but is quantitatively not correct. To compare quantitative results with Abaqus, more modes have to be taken into account. However, this cannot be done with the current model due to computational restrictions. Therefore a second version of the tire model is created with a coarser mesh. Instead of using 100 segments in the circumference only ten segments are used. See figure 6.1. Hence the maximum number of modes is reduced significantly, and quantitative results can be compared. The material parameters used for this model are the same as before and can be found in tabel B.2 in the appendix. To avoid confusion, the tire model discussed in chapter 2 will be indicated as the full tire model (100 segments), whereas the tire model discussed here will be indicated as the simplified tire model (10 segments).

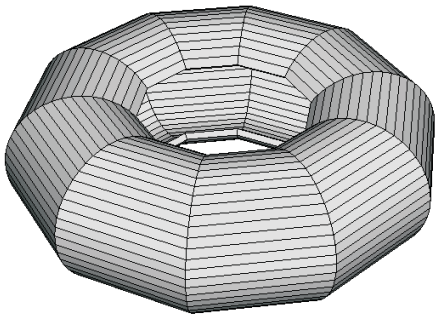

Figure 6.1: Simplified tire model, containing only ten segments.

6.1.3 Influence of the number of modes

The implemented model is a modal based model, hence it is expected that differences will occur when comparing the modal model with a model containing the full system of equations. These differences can be divided into two main sources. The first source is due to the material damping that is neglected in a modal model. Hence modal damping has to be introduced. The second source comes from the fact that only a limited number of modes (mostly small compared to the total number of modes) is used in the model. As a consequence the stiffness of the model is changed. To cope with this second source residual flexibility can be used. However, to use residual flexibility the stiffness matrix or all the modes have to be known. The latter can become a computational restriction when large FE models are used. To display the benefit of residual flexibility a simulation with the simplified tire model is made. For this simulation 100 modes are used since the interest is only to show the effect of residual flexibility. This simulation is compared with a simulation of only ten modes with and without residual flexibility. To incorporate residual flexibility (6.1) and (6.2) are used, see de Kraker [2000].

$$\mathbf{Q} \simeq \mathbf{\Phi}_k[(\mathbf{V}_{kk} - \omega^2\mathbf{I}_{kk})^{-1}\mathbf{\Phi}_k^T\mathbf{B}] + \mathbf{G}_{res}\mathbf{B} \tag{6.1}$$

$$\mathbf{G}_{res} = \mathbf{\Phi}_d\mathbf{V}_{dd}^{-1}\mathbf{\Phi}_d^T \tag{6.2}$$

Here the subscript k stands for 'kept' which are the used modes, and the subscript d stands for 'deleted' (these are the 90 modes from which the residual flexibility is taken). The matrix $\mathbf{B}$ contains all the loads, matrix $\mathbf{G}_{res}$ is the residual flexibility matrix and the vector $\mathbf{Q}$ contains the complex response. The matrix $\mathbf{V}$ and $\mathbf{\Phi}$ contain the eigenvalues and eigenvectors respectively.

In this case the residual flexibility is taken form the 90 modes that are not taken into account. Also the assumption is made that no rigid body modes occur. Remember that not the total residual flexibility is calculated since not all the modes are taken into account. The benefit of residual flexibility can be seen in (6.1) which shows that not all the modes have to be used in the online calculation. Hence the residual flexibility can be determined in front, which is computational efficient. Hereupon, if the stiffness matrix is known not all the modes have to be determined which could be efficient.

Figure 6.2 shows the results. It can be clearly seen that there is a shift when less modes are used, or when residual flexibility is neglected. The physical interpretation of the shift is that the stiffness of the structure increases as the shift becomes larger. Note that the value on the y axes is one divided by the stiffness.

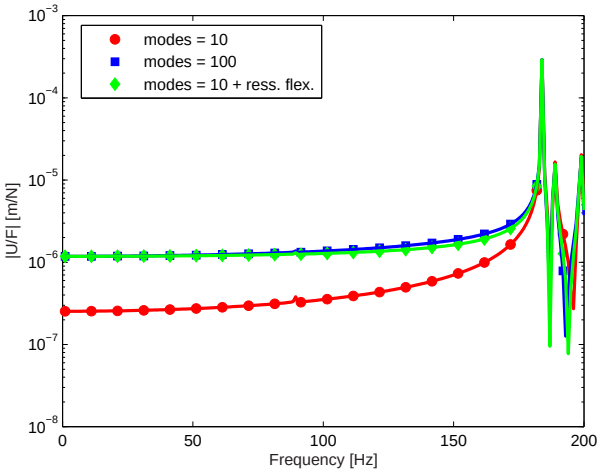

Figure 6.2: Comparison of a frequency response function for the simplified tire model, with and without residual flexibility

6.2 Validation of the modal tire vibration model

Before the tire/road contact model is validated, the modal tire vibration model is validated in the time domain. To do this the simulation results will be compared quantitatively with a simulation of Abaqus. Although these simulations are non-linear, while a modal based simulation (as the implemented model) is linear, they can be used since the deformation is very small and a linear response can be assumed.

To validate the time response of the model, the simplified tire model is subjected to a sinusoidal point force of 1 newton, with a frequency of 5 Hz. The response on the point where the force is applied is shown in figure 6.3. It can be seen that the number of modes included in the calculation has a significant influence on the time response. The reason for this can be found in the residual flexibility. Since not all of the modes are taken into account the stiffness of the tire will increase. Hence the tire will deform less for the same point force. See also the previous subsection on the discussion of full models and modal models. Taking 1000 modes it can be seen that the results agree with Abaqus. Remember however that the simplified tire model is used containing a course mesh. Also the tire model does not represent a real tire and a real tire could give other results with respect to the used modes. In this simulation a time step of 1e-5 s is used to obtain the correct results. This is necessary to model the Green's functions correctly which can be motivated in the following way: the highest eigenfrequency is the one of mode 1000, and is almost 4000 Hz. Hence the Nyquist frequency becomes 8000 Hz and Δt may be at most 1.25e-4 s. Since enough time points are needed to describe the response correctly, the time step has to be taken smaller than 1.25e-4 s.

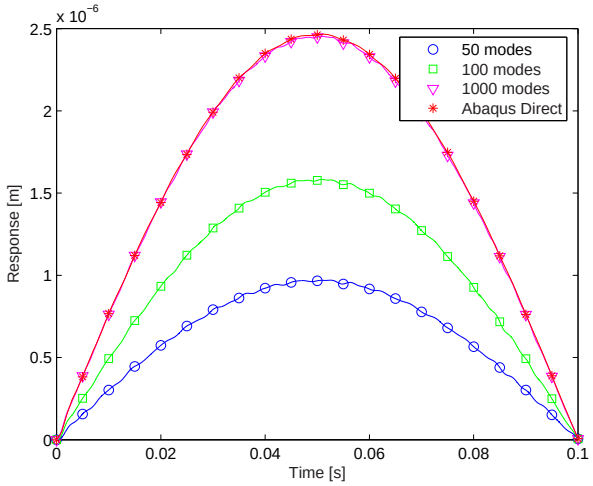

Figure 6.3: Comparison of the tire time response due to a sinusoidal point force; only the first wave of the sine is shown. Clearly visible is the influence of the number of modes taken into account (residual flexibility).

6.3 Validation of the tire/road contact model

In this section, the tire/road contact model is validated. The model that will be used is the simplified tire model with 1000 modes so that no errors are expected from the calculation of the tire response (see the previous section). To validate the contact model a flat road surface will be pressed against the tire and subjected to a given trajectory. Note that the (total) road surface will be displaced. Since it is not possible to directly calculate the contact forces in Abaqus, it is chosen to use the node displacement for validation. This is possible since it is shown that the displacement of the simplified tire model is correct with respect to the forces acting on it. Figure 6.5 displays the results where the road is displaced sinusoidal (see figure 6.4). The amplitude of the movement is 0.1 mm. The displacement in the x direction is not shown since it is close to zero and equal to the x-displacement in Abaqus. From figure 6.5 it can be seen that the displacements obtained with the contact forces show good agreement with the displacement from Abaqus. Therefore it can be concluded that the contact model gives the right contact forces. Note that some difference will always occur because the tire will always penetrate the road surface for some distance. This is necessary since the contact model needs some penetration to generate contact forces. This difference will become larger when the displacement of the road surface becomes more, but is relatively small as can be seen in figure 6.5. The parameters used for the contact model are shown in tabel B.3.

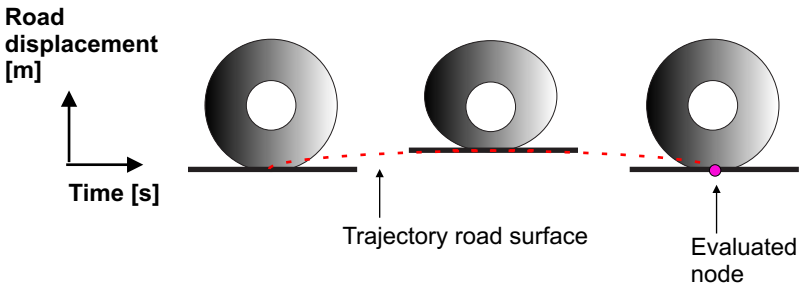

Figure 6.4: Displacement of the road surface. Note that the road surface self does not deform.

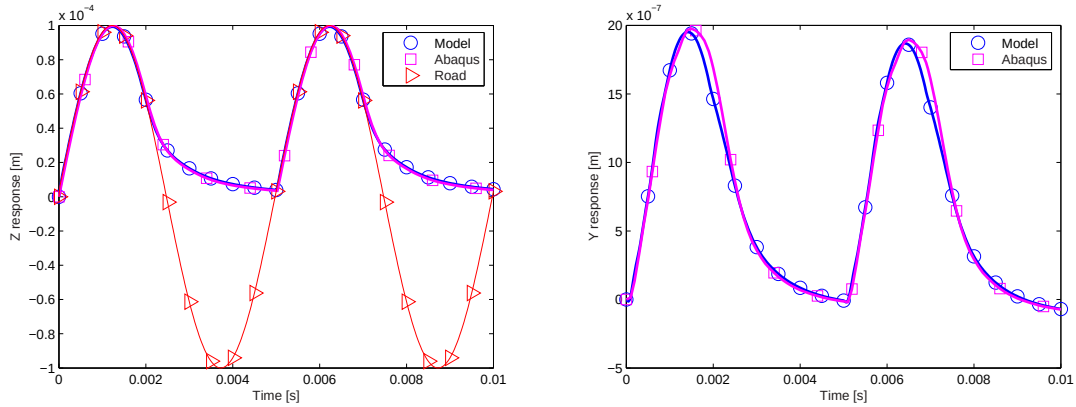

Figure 6.5: Response of the lowest tire node in contact with the road surface, see figure 6.4. Left: vertical displacement, z, right: lateral displacement,y. For this simulation the simplified tire model with 1000 modes is used, and $\gamma_1 = 500Ns/(mkg)$.

6.4 Discussion of the modelling approach

In this chapter it has been shown how Abaqus is used to validate the models. Also the necessity of using enough modes to calculate the tire stiffness correctly is discussed. For the validation of the tire model and the contact model, the simplified tire model is used so that a quantitative comparison could be made. The time responses are compared with results obtained from Abaqus, and are found to be in good agreement. It is also shown that the time step of the simulation is dependent on the eigenfrequency of the highest mode taken into account. Thus leading to a high calculation time since a large number of modes has to be used. When residual flexibility is included in the Green's functions the number of used modes, in the online calculation, can be significantly reduced as is shown in appendix C. Unfortunately appendix C also shows that the contact model gives problems using residual flexibility. Hence more research is needed.

Chapter 7

Simulation results

In this chapter simulation results obtained with the model will be discussed. First the obtained contact force distributions will be treated where the influence of rotation is discussed more extensively. Hereafter a method to obtain the axle forces will be presented, and the results obtained with this method are discussed.

7.1 Obtained contact force distributions

In this section some of the calculated contact pressure distributions obtained with the model will be discussed. Also the influence of tire rotation speed on the tire/road contact will be shown. The simulations presented in this chapter are made with the tire model described in chapter 2 (100 segments), but with altered stiffness. This is done to partly compensate for the use of a relatively small amount of modes (500 modes are used), which increases the stiffness of the structure (see chapter 6). The parameters used in these simulations can be found in tabel B.4. The tire is pressed at the road surface with 500 N, and rolls in positive x direction on a flat road surface. In this case study the (flat) road is only moved vertically, hence the horizontal deformation will be small and symmetric. Therefore, friction will not be taken into account in these simulations, and only the vertical contact forces are discussed.

7.1.1 The contact force distribution between tire/road for a non-rotating tire

In this simulation the road surface is moved 1 mm upwards, from the lowest point of the initially deformed tire. Figure 7.1 displays the contact force distribution in the contact patch for the non-rotating tire. From the results it can be seen that the distribution is symmetric with respect to both axes. This is quite logical since the tire has a symmetrical shape and is also deformed symmetrically. It can also be seen that at the sides of the contact patch the contact forces are larger than inside the contact patch. The latter observations where also done by de Beer et al. [1999], who measured the actual tire pavement contact stresses for heavy vehicles in South Africa. Hence the tire/road contact model, created in this research shows qualitatively the same results as real tire/road contact measurements.

7.1.2 The influence of tire rotating speed on the tire/road contact force distribution

In this section the influence of tire rotation speed will be discussed. For this, simulations are performed with a tire rolling on a flat frictionless road surface at different rotating speeds. As in the previous case the road surface is moved 1 mm upwards from the lowest point of the initially deformed tire.

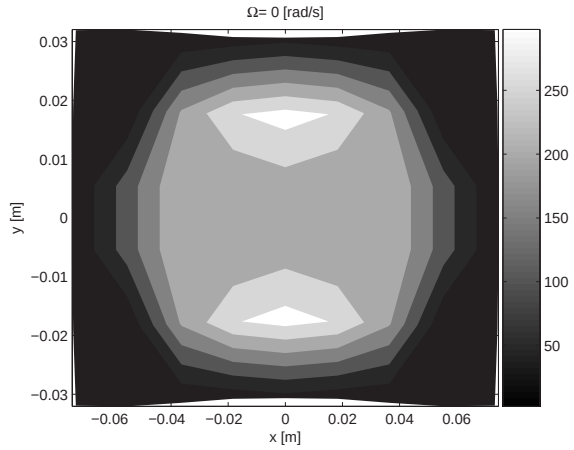

Figure 7.1: Vertical contact force distribution in the contact patch. Contact forces are in Newton's. Note that the contact forces increase at the lateral sides.

Hence a full rolling contact between tire and road is simulated by the contact model. In figure 7.2 the influence of rotation speed on the force distribution in the contact patch is shown. When the tire stands still the distribution of forces is symmetric with respect to the wheel axle. When the tire is rotating the distribution becomes asymmetric. At the front of the contact patch the forces increase. With increasing rotational speed the asymmetric behavior becomes more obvious. These observations where also made by Gong [1993], who used a two dimensional flexible ring model. The latter also shows that by increasing the internal damping of the tire the influence of rotation increases, and that if the internal damping equals zero the distribution will always be symmetric.

To investigate if this influence is also included in the model of this thesis, a second set of simulations is made. In these simulations the tire rotates with $\Omega = 150$ rad/s and the Raleigh damping coefficient γ_1 is set to respectively, 0, 2500 and 5000 Ns/(mkg). Figure 7.3 displays the results obtained from the model. It can be seen that without internal damping the pressure distribution stays symmetric, whereas with increasing internal damping the asymmetry increases. Hence the tire/road contact model gives qualitatively the same results as presented by Gong [1993].

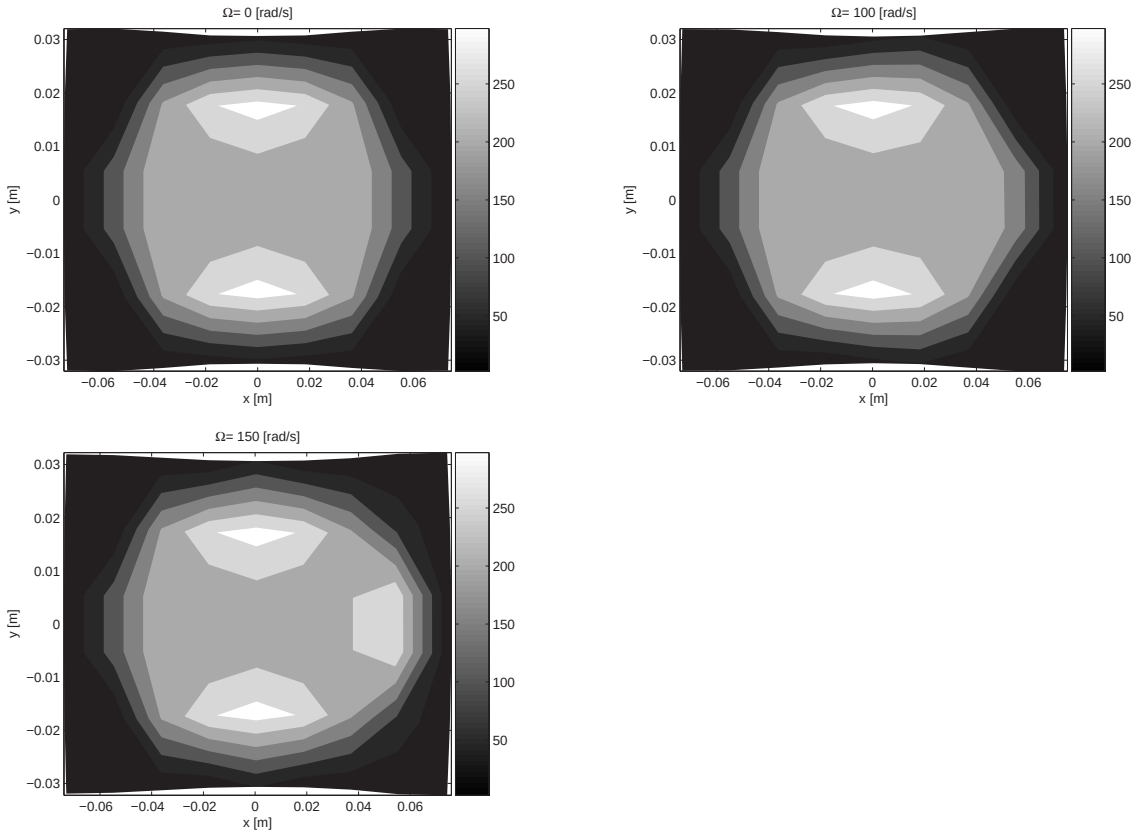

Figure 7.2: Influence of tire rotating speed on the vertical contact force distribution in the contact patch, contact forces are in Newton. Beginning in the upper left, the results are shown for $\Omega = 0$, $\Omega = 100$ *and* $\Omega = 150$ *rad/s respectively. With increasing rotational speed the distribution becomes more asymmetric.*

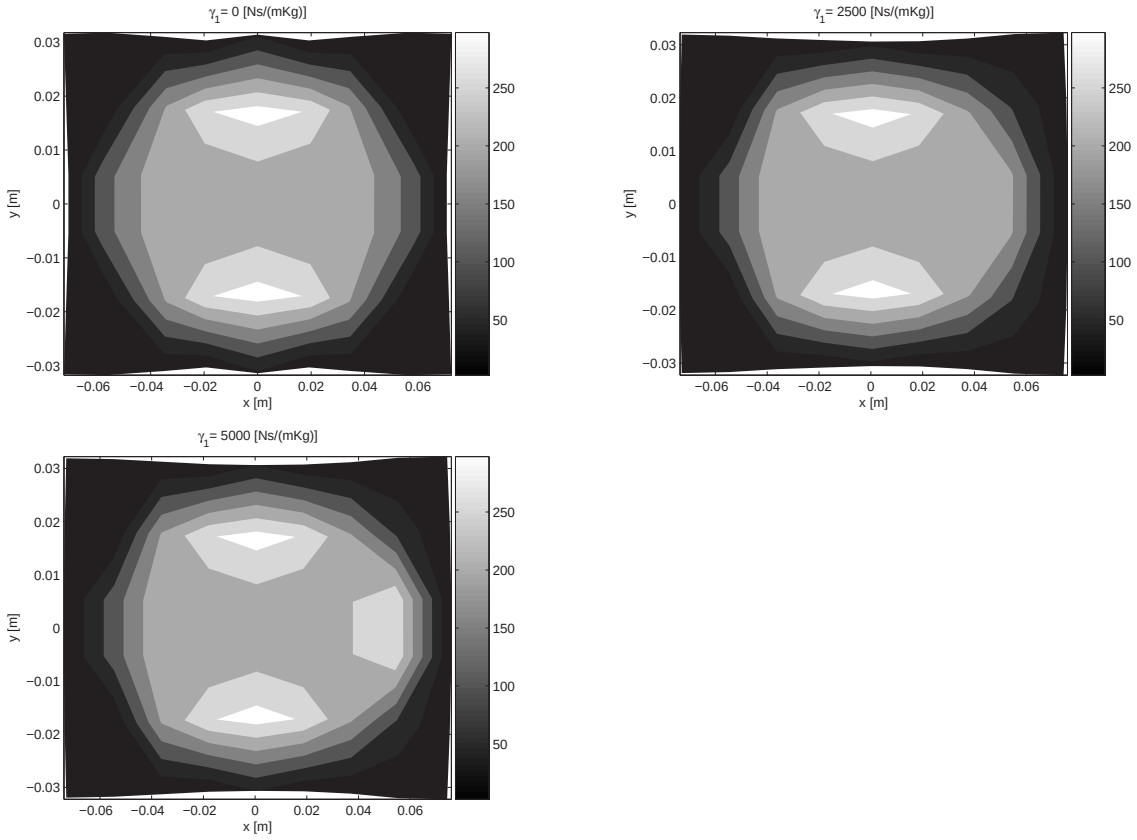

Figure 7.3: Influence of internal damping of the rotating tire ($\Omega = 150$ rad/s) on the contact force distribution; contact forces are in Newton. Beginning in the upper left, the results are shown for $\gamma_1 = 0$, $\gamma_1 = 2500$ and $\gamma_1 = 5000$ Ns/(mkg) respectively. With increasing internal damping the influence of rotation increases.

7.2 The influence of rotation on the axle forces

In the previous section the effect of rotation on the contact force distribution between the tire and the road surface is discussed and it has been shown that rotation has as significant effect. Hence the following question arises:„What is the influence of rotation on the axle forces”?. Before showing the results the method of calculation of the axle forces is briefly discussed.

The frequency response of the system can be written as follows:

$$\mathbf{x}(\omega) = \mathbf{H}(\omega)\mathbf{f}(\omega) \tag{7.1}$$

where the transfer function matrix $\mathbf{H}(\omega)$ is defined as:

$$\mathbf{H}(\omega) = \mathbf{\Phi}[-\omega^2\tilde{\mathbf{M}} + i\omega\tilde{\mathbf{D}} + \tilde{\mathbf{K}}]\mathbf{\Phi}^T \tag{7.2}$$

Here $\tilde{\mathbf{M}}$,$\tilde{\mathbf{D}}$ and $\tilde{\mathbf{K}}$ are defined as in (2.2), (2.3) and (2.5). Since there is no axle in the FE model used in this research, the axle forces are determined by the summation of all the boundary forces. These boundary forces work at the nodes located at the rim (inner circle torus, figure 2.2). These forces will be further called rim forces and the nodes, rim nodes. Taking the nodes of the contact area and the rim nodes, (7.1) can be written as:

$$\begin{bmatrix} \mathbf{x}_c(\omega) \\ \mathbf{x}_r(\omega) \end{bmatrix} = \begin{bmatrix} H_{cc}(\omega) & H_{cr}(\omega) \\ H_{rc}(\omega) & H_{rr}(\omega) \end{bmatrix} \begin{bmatrix} \mathbf{f}_c(\omega) \\ \mathbf{f}_r(\omega) \end{bmatrix} \tag{7.3}$$

Here subscript c stands for contact nodes and r for rim nodes. By assuming that the rim is infinitely stiff and does not deform, the displacement of these rim nodes can be assumed zero. Hence (7.3) can be rewritten to:

$$\mathbf{f}_r(\omega, \Omega) = \frac{-\sum \mathbf{H}_{rc}(\omega, \Omega)\mathbf{f}_c(\omega, \Omega)}{\mathbf{H}_{rr}(\omega, \Omega)} \tag{7.4}$$

This equation gives the rim forces as a function of the contact forces. The Ω dependency of $\mathbf{f}_r$ has been explicitly included in (7.4) to stress the fact that the tire rotation is included. In (7.2) can be seen that the transfer functions are dependent on the eigenvectors ($\mathbf{\Phi}$). These eigenvectors are dependent on the boundary conditions applied on the tire when the eigenvalue problem is solved. Hence when the tire is initially deformed and the rim nodes are fixed to simulate a fixed axle, no transfer function can be obtained of the rim nodes. This comes from the fact that the value of the eigenvectors for these nodes equals zero, due to the boundary condition applied (no movement). Therefore the modes of a non-deformed tire with loose rim nodes is used to calculated the transfer functions. Note that in this way also rigid body modes are included in the model, since no fixed boundary condition is applied. The tire model used for these simulations is the simplified tire model as is discussed in section 6.1.2 (the rim nodes are loose in the eigenvalue problem). The damping coefficient γ_1 is set to 0.001 Ns/(mkg). The other parameters of this tire model can be found in appendix B.2. Although this simplified tire model does not represent a realistic tire, it is sufficient to show the effect of rotation on the axle forces. For these simulations 2000 modes are used with a frequency step of 1 Hz.

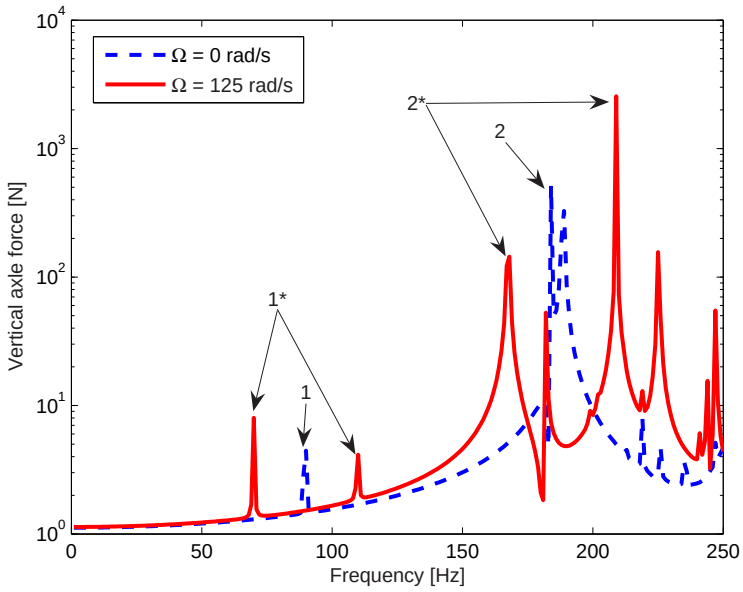

Figure 7.4: Vertical axle force. Note the shift in eigenfrequencies due to rotation. 1 and 1 indicates the second and third mode, 2 and 2* indicates the fifth and sixth mode. The * indicates the shifted eigenfrequencies.*

To show the effect of rotation on the vertical axle force, the axle forces due to a constant vertical point force are calculated. This point force works at the lowest node on the tire and has a value of 1 N. Figure 7.4 displays the results for a non-rotating tire and a tire rotating with 125 rad/sec. It can be clearly seen that the non-rotating tire shows a peak at 90 Hz and 188 Hz which are the eigenfrequency of the 2^{nd}, 3^{th} and 4^{th}, 5^{th} mode respectively. These eigenfrequencies are also calculated with Abaqus for the model with fixed rim nodes. When rotation is applied these eigenfrequencies shift, indicated with an astrix. This eigenfrequency shift is also observed in chapter 4 where the vibrational response is calculated for a rotating tire.

7.3 Summary

In this chapter only the case of a vertical contact without friction is discussed. For investigating another case with friction, the problem arises that the tire mesh is to course to give results which can be used. Defining a finer mesh is however not possible due to computational restrictions.

The obtained results show that the contact forces are not equal over the whole contact patch. Instead, they increase at the lateral sides of the contact patch. These results where also obtained in real tire/road contact measurement found in literature. With respect to the influence of rotation, the obtained results show that the contact force distribution becomes asymmetric when the tire rotates. It is also shown that internal damping has a significant influence on the contact force distribution. These observations are also found in literature.

For the axle forces a method is presented to calculated them from the obtained contact forces, including rotation of the tire. The results show that the shift in eigenfrequencies, as in the tire vibrational response, can also seen with axle forces.

Chapter 8

Conclusions and recommendations

8.1 Conclusions

At Eindhoven University of Technology a tire model for tire/road noise is under development. The aim of this master project is to improve the computational efficiency of the existing model and to implement a tire/road contact model.

A literature study, regarding tire/road contact models is performed, in which two main approaches are found. In the first approach all the contact points are considered separately without any cross correlation. In the second approach this correlation is incorporated and it is therefore a more realistic approach. From this literature study it is concluded that the vertical contact forces are modelled best using an elastic half-space. For the modelling of the horizontal forces, the literature study has shown that a brush model is generally used. Since this brush model can be well combined with the elastic half-space it is also used in this research.

Since the distribution of contact points constantly change in time the tire/road interaction is non-linear. Hence, the contact problem has to be solved in the time domain. The response of the tire to the contact forces must therefore be obtained from the convolution product of the Green's functions and the contact forces. These Green's functions can be obtained by taking the inverse Fourier transform of the frequency response functions. However, this is computationally inefficient. To calculate the Green's functions, computational efficient, a semi-analytical expression is derived which makes it possible to directly calculate the point to point, time dependent Green's function. The expression is validated and the results show that the eigenfrequency shift due to rotation is correctly predicted.

The contact problem is solved in the time domain since the contact problem is non-linear. This is done by describing the problem as an initial value problem for each time step. Validation has shown that the obtained results are correct. It is also shown that a large number of modes has to be taken into account to obtain correct results. However, since the very simplified tire model used does not represent a real tire other results with respect to the used modes will probably be obtained when using a model of a real tire.

To display the effect of rotation on the vertical axle forces, a method is presented to calculate these axle forces. The results obtained with this approach show that the axle forces also display the frequency shift due to rotation.

The presented results show that the contact force distribution in the contact patch qualitatively corresponds with measurements shown in literature. Also the effect of rotation and internal damping is correctly incorporated.

8.2 Recommendations

Although this thesis gives a valuable insight in the rolling tire/road contact, some recommendations for further research can be formulated.

- The tire model used in this research is of a very simple kind. As a consequence it does not include layers of reinforcement or a realistic shape. Also, it contains only a little number of nodes in the contact patch. One can think of making a tire model which includes reinforcement and has a relatively high number of nodes in the contact area. The challenge of this will be to validate the model response with respect to a real tire.
- A more general recommendation is to investigate the possibility to make a special test tire so that the model can be validated with real measurements.
- It is shown that the model needs a large number of modes to calculate the response correctly. By introducing a super element in Abaqus, consisting of only the nodes of interest, the number of nodes, can be reduced significantly. In that case the mass matrix and the number of nodes in $\mathbf{\Phi}$ are reduced, leading to a beter computational efficiency.
- In the initial deformation in Abaqus the horizontal forces are not incorporated. These forces can, most likely, be incorporated by determining the contact stresses and calculating from these the horizontal contact forces.
- In the appendices it is shown that not all the modes have to be taken into account in the online calculations to calculate the response correctly. However the contact model does not allow this approach. Research can be done on manners to transform the convolution integral, so that the contact model can use the Green's functions with residual flexibility.
- A third option to reduce the number of used modes is to investigate the possibility of making a "intelligent" choice on the modes that are used.
- Until now the model uses a fixed axle which is only valid in special test cases. By allowing the axle to move in for example a suspension system, the model can be used in realistic operating conditions.

Bibliography

R. Blom. Modelling tyre vibrations - a modal approach. Master's thesis, Eindhoven University of Technology, Eindhoven, the Netherlands, 2005.

A. Burke and O. Olatunbosun. Static tyre/road interaction modelling. *Meccanica*, 32:473–479, 1997.

M. de Beer, L. Kannemeyer, and C. Fisher. Towards improved mechanistic design of thin asphalt layer surfacings based on actual tire/pavement contact stress - in - motion (sim) data in south africa. In *Proc. of the 7th conference on asphalt pavements for South Africa*, 1999.

B. de Kraker. *A Numerical-Experimental Approach in Structural Dynamics*. Eindhoven University of Technology, Eindhoven, the Netherlands, 2000.

B. de Kraker and D. van Campen. *Mechanical vibrations*. Shaker Publishing BV, 2000. ISBN 90 423 0165 1.

T. Fujikawa, A. Funazaki, and S. Yamazaki. Tire tread temperature in actual contact areas. *Tire science and technology*, 22(1):19–41, 1994.

T. Fujikawa, H. Koike, Y. Oshino, and H. Tachibana. Definition of road roughness parameters for tire vibration noise control. *Applied Acoustics*, 66:501–512, 2005.

S. Gong. *A study of in-plane dynamics of tires*. Delft University of Technology, Delft, the Netherlands, 1993. ISBN 90 370 0092 4.

R. Hayden. Roadside noise from the interaction of a rolling tyre with road surface. In *In Proc. Of the purdue Noise Control conference, Purdue University, Indiana, USA*, 1971.

D. Hill, D. Nowell, and A. Sackfield. *Mechanics of Elastic Contacts*. Butterworth-Heinemann Ltd, 1993. ISBN 0 7506 0540 5.

K. Johnson. *Contact Mechanics*. Cambridge University Press, Cambridge, England, 1985. ISBN 0 521 25576 7.

Y. Kim and J. Bolton. Modeling tire treadband vibration. In *Proceedings of Internoise 2001 27-30 August, The Hague, Netherlands*, 2001.

W. Kropp. A mathematical model of tyre noise generation. *Heavy Vehicle Systems, Int. J. of Vehicle Design*, 6(1-4):310–329, 1999.

W. Kropp, K. Larsson, F. Wullens, P. Andersson, and F. Becot. The generation of tyre/road noise - mechanisms and models. In *ICSV 10 7-10 July 2003, Stockholm, Sweden*, 2003.

K. Larsson. A rolling contact model using green's functions. In *InterNoise 29 27-30 August 2000, Nice, France*, 2000.

K. Larsson and W. Kropp. A high-frequency three-dimensional tyre model based on two coupled elastic layers. *Journal of sound and vibration*, 253(4):889–908, 2002.

I. Lopez, S. Kersjes, N. Roozen, A. Schmeitz, and H. Nijmeijer. Green's functions for a rotating tyre: a semi-analytical approach. In *Euronoise 2006, 30 May - 1 June, Tampere, Finland*, 2006.

A. Love. The stress produced in a semi-infinite solid by pressure on part of the boundary. *Philosophical transactions of the Royal Society of London*, 228:377–420, 1929.

F. Mancosu and D. Minen. Non-linear modal rolling tyre modeal for dynamic simulation with adams. In *European Adams User Conference 18-19 november 1998, Paris, France*, 1998.

U. Sandburg and J. Esjmont. *Tyre/Road noise refernece book*. Informex SE-59040 Kisa, Sweden, 2002.

F. Wullens and W. Kropp. A three dimensional rolling contact model for the description of the tyre/road interaction. In *ICSV 10 7-10 July 2003, Stockholm, Sweden*, 2003.

F. Wullens and W. Kropp. A three-dimensional contact model for tyre/road interaction in rolling conditions. *Acta Acustica united with Acustica*, 90:702–711, 2004.

Appendix A

Tire noise generation mechanisms

As said before tire noise generation mechanisms are subject of research for more than 30 years. This research has led to a complicated mixture of mechanisms. All of these mechanisms are commonly accepted by most experts, and there is no disagreement in the existence of them. There is, however, no clear consensus about the importance of these mechanisms.

This section will briefly describe the, generally accepted, tire noise mechanisms, which can be divided into two main categories: Mechanical mechanisms (occur mostly below 1000 Hz) and Aerodynamical mechanisms (occur mostly above 1000 Hz). Also Amplification mechanisms will be discussed, and although these mechanisms are not real noise producing mechanisms, they can have an important influence on the production of tire/road noise. Much information is taken from Sandburg and Esjmont [2002] to which the reader is referred for a more detailed description of the mechanisms.

A.1 Mechanical mechanisms

Radial vibrations
Time varying contact forces due to tread impact (300-1500 Hz), surface roughness deflecting the tire (800-1250), and rolling deflection will cause radial tire vibrations. It is believed that up to 1000 Hz these vibrations dominate the noise generation. The vibrations will also propagate to the sidewalls, where radiation of the sidewalls dominates between 400 and 600 Hz. It may be clear that each non-uniformity, as road roughness or non-roundness, will cause these vibrations. Hence this mechanism is of most interest in this research.

Stick/Slip and stick/snap
This mechanism is related to friction and adhesion. Stick/slip occurs when tread elements are passing through the contact patch. Here they will gather potential energy until the forces exceed the maximum friction forces. At this point the tread element slips back to a position in which the friction forces and potential energy, in the tread element, are in equilibrium. Stick/slip is considered to play an important role when large tangential forces act on the tire, as occurs when braking or cornering. During free rolling this mechanism is considered to be much less important. Stick/Snap is more related to adhesion of the tread elements, and occurs when a tire becomes ”sticky”. To break the adhesion of the tread elements with the surface a stretching force will act, hence the tread elements will vibrate when the adhesion is broken. The stick/snap mechanism is not considered to be very important for traffic noise, since the road surface is usually covered with dirt. However, when testing a tire on a clean drum it could be important.

A.2 Aerodynamical mechanisms

Flow induced noise
A rotating tire will induce turbulence in the air surrounding the tire. However, the noise generated by this mechanism only has a significant contribution at speeds well above normal highway speeds. Hence this mechanism is not important for tire/road noise calculations during normal (car) driving speeds.

Air pumping
A rolling tire will enclose, in its contact patch, a volume of air within the cavities and pores constituted by the tread pattern and surface texture. In the front of the contact patch the air is compressed and pressed away, while it is sucked and expands at the rear. Due to variations of surface texture and tire deformation, the tread pattern grooves will be squeezed. Thus the

air flow will change in time. This generates vibrations in the surrounding air and therefore constitutes a source of sound, characterized by the volume change per unit time. Hayden [1971] first presented the air pumping theory, where the volume flow at the contact patch is modelled in a rather simple way, as a monopole source.

A.3 Amplification mechanisms

Although amplification mechanisms are no real noise mechanisms they have an important influence on tire/road noise. Hence the three most important mechanisms will be discussed in the following sections.

Horn effect
Close to the leading and trailing edges of the tire footprint, the tire and the road surface form a structure with a narrow ”throat” at the edges, which widens more and more the further out from the edges one moves. This geometry provides a better match between the impedance at the ”throat” (where a major part of the noise is generated) and the ambient acoustical impedance. The amplification starts at 300 Hz and may reach up to 1.5 - 2 kHz.

Torus cavity resonance
The air column in the tire cavity can resonate at a certain frequency. The frequency of the cavity resonance is defined only by the tire and rim size and the speed of sound in the medium that inflates the tire. A simplified equation for the cavity resonance frequency is:

$$f = \frac{c}{l_{cav}} = \frac{2nc}{\pi(D_{cav} + d_{cav})}[Hz] \tag{A.1}$$

c : speed of sound in the gas inflating the tire [m/s]
l_{cav} : length of the cavity [m]
D_{cav} : outer diameter of the cavity [m]
d_{cav} : inner diameter of the cavity [m]
n : integer
Typical frequencies for passenger car tires are in a range of 220-280 Hz (n=1), depending on the tire size. This means this resonance is more important for interior noise than for exterior noise.

Appendix B

Model parameters used in this thesis

nodes	7600	[-]
elements	100	[-]
E_{tire}	480	[MPa]
ν_{tire}	0.45	[-]
ρ	1200	[kg/m^3]
γ_1	0.001	[Ns/mkg]
γ_2	0	[s/kg]

Table B.1: Tire parameters used for the full tire model

nodes	760	[-]
elements	10	[-]
E_{tire}	480	[Mpa]
ν_{tire}	0.45	[-]
ρ	1200	[kg/m^3]
γ_1	5000	[Ns/mkg]
γ_2	0	[s/kg]

Table B.2: Tire parameters used for the simplified tire model

Ω	0	[rad/s]
Modes	1000	[-]
γ_1	5000	[Ns/mkg]
γ_2	0	[s/kg]
K_b	199620	[N/m]
E_{ehs}	340	[MPa]
ν_{ehs}	0.49	[-]
ξ	0.75	[-][
Δt	2.5e-5	[s]

Table B.3: Model parameters used in the validation of the contact model

$nodes$	7600	[-]
$elements$	100	[-]
Modes	500	[-]
γ_1	5000	[Ns/mkg]
γ_2	0	[s/kg]
E_{tire}	48	[MPa]
ν_{tire}	0.45	[-]
ρ	1200	[kg/m^3]
E_{ehs}	340	[MPa]
ν_{ehs}	0.49	[-]
ξ	0.75	[-][
Δt	2.5e-5	[s]

Table B.4: Parameters used for the presented results

Appendix C

Introducing residual flexibility in the Green's functions

In this thesis it is shown that residual flexibility can be used to reduce the necessary number of modes. Hence, if this can be included in the semi-analytical expression of the Green's function, great progress in online calculation time can be achieved. Therefore this appendix will discuss the introduction of residual flexibility in the semi analytical expression of the Green's functions. For the complete derivation of the Green's functions it is referred to chapter 4.

For a system with non-symmetric matrices the frequency response function can be described according to:

$$H(\omega) = \sum_{k=1}^{m} \frac{\mathbf{u}_{ik}\mathbf{w}_{jk}}{-s_k + s} \tag{C.1}$$

where **u** and **w** are the matrices of eigenvectors from the right and left eigenvalue problems respectively. s_k are the eigenvalues of the right eigenvalue problem. If $s << s_k$ (C.1) can be written as,

$$H(\omega) = \sum_{k=1}^{n} \frac{\mathbf{u}_{ik}\mathbf{w}_{jk}}{-s_k + s} + \sum_{k=1+n}^{m} \frac{\mathbf{u}_{ik}\mathbf{w}_{jk}}{-s_k} \tag{C.2}$$

Performing an inverse Laplace transformation on (C.2) results into:

$$h(t) = \sum_{k=1}^{n} \mathbf{u}_{ik}\mathbf{w}_{jk}e^{s_k t} + \sum_{k=1+n}^{m} \frac{-\mathbf{u}_{ik}\mathbf{w}_{jk}}{s_k}\delta(t) \tag{C.3}$$

Here n indicates the modes which are kept from the total number of modes m. The $\delta(t)$ can be replaced by $\frac{1}{\Delta t}$ at $t = 0$. Using the same approach for the Green's functions as displayed in chapter 4, (4.14) changes into:

$$g_{ij}(t=0) = \sum_{k=1}^{m} \Phi_i^k \left[\sum_{q=1}^{2n} U_k^q \frac{\sum_p^m w_p^q \Phi_j^p}{a_q} e^{s_q t} \right] + \frac{\sum_{k=1}^{m} \Phi_i^k \left[\sum_{q=2n+1}^{2m} U_k^q \frac{\sum_p^m -w_p^q \Phi_j^p}{a_q} \frac{1}{s_q} \right]}{\Delta t} \tag{C.4}$$

$$g_{ij}(t>0) = \sum_{k=1}^{m} \Phi_i^k \left[\sum_{q=1}^{2n} U_k^q \frac{\sum_p^m w_p^q \Phi_j^p}{a_q} e^{s_q t} \right] \tag{C.5}$$

Since the last part of (C.4) is constant it can be determined before the actual simulation starts. Also less modes are used in the online calculation which has as benefit that the time step can become larger since the frequency of the modes decreases (See section 6.2). Hence, great progress in calculation time can be achieved.

To validate the response obtained with (C.4) and (C.5), the simplified tire model is subjected to a sinusoidal point force of 20 Hz with an amplitude of 1 N. In this simulation 100 modes are used with γ_1 = 50 Ns/(mkg). To calculate the residual flexibility 90 modes, only 10 modes are kept, are used. The results are shown in figure C.2. In the right figure the response is plotted. The left figure displays the Green's functions where it can clearly be seen that at t=0 a constant is added.

The shown results validate the possibility to use residual flexibility in the calculation of the system's response to a predefined force. It also shown that the Green's functions are completely different, especially at t=0. As a consequence the contact model, which uses the value of the green's function on t=0, calculates other contact forces. Hence the response is also different, and it has to be concluded that as long as the contact model uses the Green's function, residual flexibility can not be used.

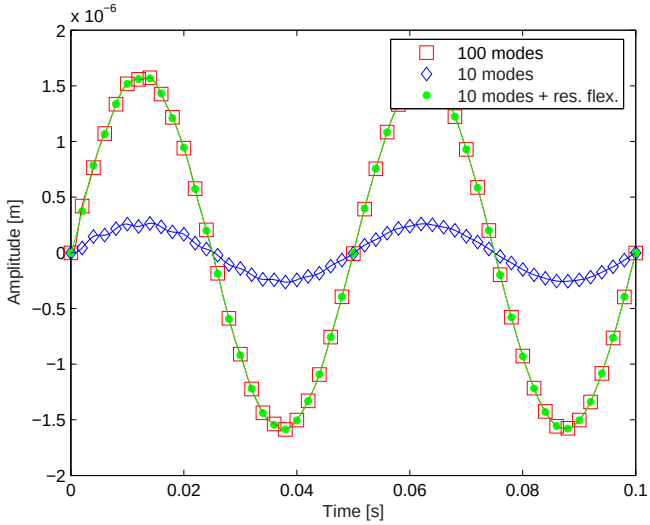

Figure C.1: Tire response to a sinusoidal point force. For this simulation 100 modes are used with $\gamma_1 = 50Ns/(mkg)$*. Note that the amplitude of the response without residual flexibility is smaller due to the increased stiffness.*

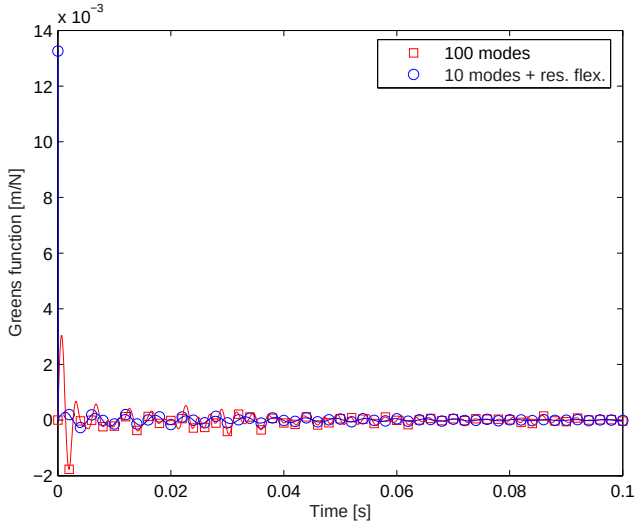

Figure C.2: Green's functions for 100 modes and 10 modes with residual flexibility. Note the peak at t=0.

Appendix D

1 dof example calculating the Green's function

This example concerns a 1 dof system, it may therefore be clear that the stiffness and damping matrices are always symmetric and diagonal. Nevertheless it will only be used to demonstrate the basics of the theory. The mass stiffness and damping are assumed to have the value 1, so the system equation is defined as.

$$\ddot{u}(t) + \dot{u}(t) + u(t) = F(t) \tag{D.1}$$

Solving the first eigenvalue problem,it may be obvious that the eigenvector and eigenfrequency are 1, since the stiffness and mass are 1. Hence the damping and stiffness remain the same in modal coordinates, as $d^* = \Phi d \Phi = d$. Writing the system equation in modal coordinates with $x(t) = \Phi\eta(t)$ it becomes

$$\ddot{\eta}(t) + \dot{\eta}(t) + \eta(t) = \Phi F(t) \tag{D.2}$$

Transforming the system from second order to first order, as proposed by de Kraker and van Campen [2000], it becomes.

$$\begin{bmatrix} 1 & 1 \\ 1 & 0 \end{bmatrix} \begin{bmatrix} \dot{\eta}(t) \\ \ddot{\eta}(t) \end{bmatrix} + \begin{bmatrix} 1 & 0 \\ 0 & -1 \end{bmatrix} \begin{bmatrix} \eta(t) \\ \dot{\eta}(t) \end{bmatrix} = \begin{bmatrix} F(t) \\ 0 \end{bmatrix} \tag{D.3}$$

Solving the second eigenvalue problem the eigenvalues and eigenvectors become for the right as well as the left eigen value problem.

$$\mathbf{U} = \begin{bmatrix} -0.56 - 0.44i & -0.56 + 0.44i \\ 0.66 - 0.27i & 0.66 + 0.27i \end{bmatrix}, \mathbf{S} = \begin{bmatrix} -0.50 + 0.87i & 0 \\ 0 & 0.50 - 0.87i \end{bmatrix} \tag{D.4}$$

Here $\mathbf{U}$ are the eigenvectors and $\mathbf{S}$ the eigenvalues. Note that $\mathbf{S} = \lceil s_r \rfloor$. Substituting this in (4.14), the green's function becomes.

$$\begin{aligned} h_{ij}(t) = & \\ & (-0.56 - 0.44i)\frac{(-0.56 - 0.44i)}{(-0.85 + 0.22i)} e^{(-0.50+0.87i)t} \\ & + (-0.56 + 0.44i)\frac{(-0.56 + 0.44i)}{(-0.85 - 0.22i)} e^{(-0.50-0.87i)t} \end{aligned} \tag{D.5}$$

A graphical representation of (D.5) is displayed in figure D.1.

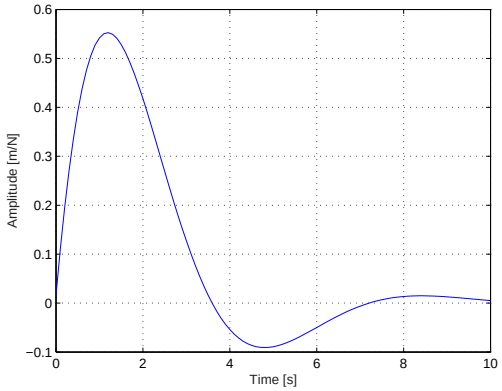

Figure D.1: Graphical representation of the Green's function from this example.

Appendix E

Uniform pressure applied to a rectangular area

For this discussion the book of Johnson [1985] is mostly used, and for more detailed information it is referred to this book.

The classical approach to finding the stresses and displacements in an elastic half-space due to surface traction is due to Boussinesq(1885) and Cerruti(1882) who made use of the potential theory. Love [1929] applied this potential theory to describe the stress and displacement in the elastic half-space for important, special problems such as rectangular and circular areas under uniform pressure. Although discussing the total derivation of the formula's create by Love [1929] is beyond the scope of this research, the main assumptions and approach on the derivation of the formula used in this research, will be treated. For more information is referred to, Love [1929], Johnson [1985] and Hill et al. [1993]. Figure E.1 shows a rectangular contact patch of dimensions 2a x 2b, centered on the origin. On this contact patch a uniform pressure P_0 acts, hence the boundary conditions of the pressed area are $z = 0$, $x = \pm a$, $y = \pm b$. The approach will be direct application of the potential theory as described in Hill et al. [1993] chapter 12. Briefly spoken, the state of stress within a elastic half-space may de obtained from two potentials ψ and ψ_1 chosen such that the boundary conditions are correctly represented. In the case of a body under normal pressure alone it is possible to write down simple forms of ψ and ψ_1 assuming that the pressure is constant.

$$\psi_1 = P_0 \int\int \chi \, dr\, ds \tag{E.1}$$

$$\psi = P_0 \int\int \frac{dr\, ds}{R} \tag{E.2}$$

Where

$$\chi = ln(R + z) \tag{E.3}$$

$$R^2 = (x - r)^2 + (y - s)^2 + z^2 \tag{E.4}$$

In principle, both of the above equations could be evaluated first, and used as the starting point for the solution of the pressure/displacement distribution in the elastic half-space. However from the formulas used to obtain the displacement and stresses it can be noticed that only the derivatives of ψ_1 appear, and it is therefore unnecessary to evaluate the function itself. Instead (E.1) is differentiated within the integral sign resulting in:

$$\frac{\psi_1}{dx} = P_0 \frac{d}{dx} \{ \int\int \chi \, dr\, ds \} \tag{E.5}$$

For the rectangular contact this becomes.

$$\frac{\psi_1}{dx} = \int_{-b}^{b} [ln(z + r)]_{-a}^{a} ds \tag{E.6}$$

A similar approach can be used to find $\frac{\psi_1}{dy}$. The algebra involved in carrying out the previous equations is lengthy but gives explicit results. Many of these results have been found by Love [1929]. The result of the potential ψ is.

$$\begin{aligned} \frac{\psi}{P_0} = {} & (y + b) ln \frac{x + a - \gamma}{x - a + \delta} - (y - b) ln \frac{x + a - \beta}{x + a - \alpha} \\ & + (x + a) ln \frac{y + b + \gamma}{y - b + \beta} - (x - a) ln \frac{y + b + \delta}{y - b + \alpha} \\ & + 2z(\theta_C - \theta_D + \theta_A - \theta_B) \end{aligned} \tag{E.7}$$

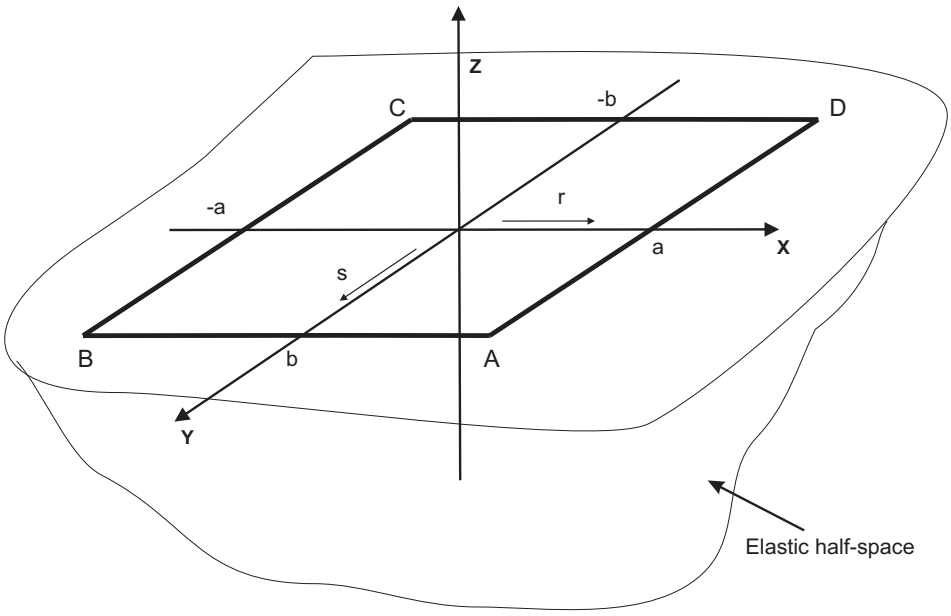

Figure E.1: A elastic half-space

Where

$$\begin{aligned}\alpha^2 &= (x-a)^2 + (y-b)^2 + z^2 \\ \beta^2 &= (x+a)^2 + (y-b)^2 + z^2 \\ \gamma^2 &= (x+a)^2 + (y+b)^2 + z^2 \\ \delta^2 &= (x-a)^2 + (y+b)^2 + z^2 \end{aligned} \tag{E.8}$$

$$u_z = \frac{1}{4\pi E}[2(1-\nu)\psi - z\frac{d\psi}{dz}] \tag{E.9}$$

For the description of $\theta_{A..D}$ is referred to Hill et al. [1993], since these will not be used here. Note that in (E.8) the quantities α, β, γ, δ represent respectively the distances from the point (x, y, z) to the corners A, B, C, D of the contact patch (figure E.1). For the instance of a punch, the normal displacement of the surface can be found from (E.7), (E.8) and (E.9), simply by setting z=0. (E.9) gives the displacement in the elastic half-space as a function from the potential (see Hill et al. [1993]). This substitution results in:

$$\begin{aligned}\frac{\pi E}{1-\upsilon^2}\frac{\Delta u_z}{p} = & \\ &+ (x+a)ln\frac{(y+b)+\sqrt{(y+b)^2+(x+a)^2}}{(y-b)+\sqrt{(y-b)^2+(x+a)^2}} \\ &+ (y+b)ln\frac{(x+a)+\sqrt{(y+b)^2+(x+a)^2}}{(x-a)+\sqrt{(y+b)^2+(x-a)^2}} \\ &+ (x+a)ln\frac{(y-b)+\sqrt{(y-b)^2+(x-a)^2}}{(y+b)+\sqrt{(y+b)^2+(x-a)^2}} \\ &+ (y-b)ln\frac{(x-a)+\sqrt{(y-b)^2+(x-a)^2}}{(x+a)+\sqrt{(y-b)^2+(x+a)^2}}\end{aligned} \tag{E.10}$$

With this equation the z displacement of the elastic half-space at coordinate (x, y), due to an uniform pressure acting at a rectangular surface, can be determined. Here E and ν are the Youngs modulus and the Poissons ratio of the elastic half-space.